**DOI: https://doi.org/10.15407/pmach2022.02.038**

UDC 627.7

# EFFECT OF VARYING HEAT TREATMENT REGIMES ON MICROSTRUCTURE AND MECHANICAL PROPERTIES OF P92 STEEL WELDS

**Vinay Kumar Pal**
gaurishankar.vinaypal@gmail.com
ORCID: 0000-0001-7830-570X

**Lokendra Pal Singh**
ORCID: 0000-0002-6221-8174

Department of Mechanical Engineering,
Sam Higginbottom University
of Agriculture, Technology and Sciences
Allahabad, 211 007, Uttar Pradesh, India

*Cr-Mo steels are well-known for their high temperature application in thermal power plants. P91, P911 and P92 are most commonly used Cr-Mo steels for high temperature application. The steels derived their strength from tempered martensite and precipitates of MX and $M_{23}C_6$ type. The normalizing and tempering of the steels are performed before putting them in service condition. The present manuscript describes the effect of the varying heat treatment regimes on microstructure and mechanical properties of the P92 steel. The normalizing effect on microstructure and mechanical properties has been studied. The normalizing was performed in the range of 950–1150 ºC. The effect of the varying tempering time on mechanical behavior of the P92 steel has also been studied and effort to develop relation between microstructure and mechanical properties was made. Optical microscope and scanning electron microscope have been utilized for microstructure study. To characterize the mechanical behavior, tensile, hardness and Charpy impact toughness tests were performed.*

***Keywords:*** *P92, microstructure, mechanical properties, normalizing, tempering.*

## 1 Introduction

P92 steel is commonly employed for USC and AUSC power plants for components that have operating temperatures in the range of 550–620 ºC. At such high temperature material undergoes several microstructural changes, which ultimately affect the mechanical properties of the material. The degradation in mechanical properties results in the failure of the components. High-temperature mechanical strength of the P92 steel depends on the microstructure and mechanical properties of the virgin steel, i.e. before putting in service condition. The strength of P92 steel in a virgin state is derived from the solid solution and precipitate strengthening, which are derived from varying heat treatments. Hence, it becomes necessary to study the effect of varying heat input on the microstructure and mechanical properties of P92 steel. P92 steel was developed by adding strong carbide and carbonitride forming elements, such as 0.2 wt.% vanadium, 0.08 wt.% niobium, and 0.05 wt.% nitrogen [1] in P9 steel. P92 steel is processed tempered martensitic microstructure obtained by normalizing and tempering treatment (N&T). Normalizing of P91 steel is generally carried out in the austenitizing temperature range of 1040–1060 ºC for 20–40 min, followed by air cooling. The subsequent tempering is performed in the temperature range of 730–780 ºC for 1–2 h, followed by air cooling. The strength of P92 steel is primarily derived from its stable microstructure. The stability of microstructure is governed by the tempered martensitic lath structure, sub-grain size, prior-austenite grain boundaries (PAGBs), lath width, lath boundaries, precipitates size and their distribution inside the structure, dislocation density, precipitates morphology and their amount [2]. Presence of high dislocation density, pinning of precipitates like Cr-rich $M_{23}C_6$ [M: Cr, Fe, Mn, Mo], V and Nb-rich MX and solute atom, result in a large driving force required for recovery that produces a stable structure as required for high creep strength. The mechanical properties of P92 steel are governed by the solid solution hardening, sub-grain size hardening, and precipitation hardening. The microstructure and mechanical properties of P91 steel were found to be more sensitive to normalizing and tempering temperature and time.

Shrestha et al. [3] studied the effect of varying normalizing temperature (1020–1100 ºC), normalizing time (2–8 h), tempering temperature (690–790 ºC), tempering time (2–20 h) on microstructure evolution and hardness of P912 steel. Martensitic lath size and PAGs size were observed to be increased with increase in normalizing temperature (fixed normalizing time) and time (fixed normalizing temperature). The hardness

of steel was found to decrease with increase in normalizing temperature and time. The hardness of P92 steel was reported to decrease with an increase in tempering temperature to lower critical temperature ($A_{c1}$). The reactions associated with thermal phase transformation for $A_{c1}$, $A_{c3,}$ 1270 ºC temperatures are given below

$$\alpha + M_{23}C_6 + (V,Nb)(C,N) \rightarrow \alpha + M_{23}C_6 + (V,Nb)(C,N) + \gamma \qquad 820\,(A_{c1})^{\circ}C; \tag{1}$$

$$\alpha + \gamma + M_{23}C_6 + (V,Nb)(C,N) \rightarrow \gamma + (V,Nb)(C,N) \qquad 870\ (A_{c3})^{\circ}C\ ; \tag{2}$$

$$\gamma + (V,Nb)(C,N) \rightarrow \gamma + \delta + Nb(C,N) \qquad 1270\,^{\circ}C\,. \tag{3}$$

The dissolution of $M_{23}C_6$ precipitates started above $A_{c1}$ temperature and was found to be completed at $A_{c3}$ temperature. V-rich MX precipitates also dissolved at a temperature of 1270 ºC. The dissolution of precipitates results in the higher availability of C and N in a matrix, which led to increase in solid solution strengthening. Effect of varying normalizing temperature (1010–1100 ºC) and tempering temperature (730–780 ºC) on microstructure evolution and mechanical properties was performed by Golañski [4]. Strength properties were reported to be optimum in normalizing temperature range of 1010–1040 ºC, while optimum plastic properties like Charpy toughness and ductility were obtained in the temperature range of 1070–1100 ºC. Increase in tempering temperature from 730 ºC to 780 ºC led to a reduction in strength and increase in plastic properties. Golañski and Słania [5] have reported similar results for the cast and forged P91 steel. Jones et al. [6] have studied the effect of cooling medium and varying tempering temperature (650–760 ºC) on precipitate evolution. Annealing of the tempered sample was also performed for varying annealing temperature (550–650 ºC) and time of 1000 h. In air-cooled condition, coarse lath structure was obtained clearly due to slow cooling rate. In water-quenched condition, microstructure was found to be free from precipitates except for residue precipitates of NbC and $(Fe, Cr)_3C$ that remain undissolved during normalizing. For low tempering temperature of 550 ºC, hardness remains unaffected by tempering time, while at higher tempering temperature, hardness decreased continuously with increase in tempering time and stabilized after 1 h. V-rich V-Cr-Nb precipitates were observed just after 16 min of tempering at 760 ºC. Cr-rich Cr-V-Fe precipitates were observed after 16 min of tempering and converted to more stable Cr-rich $(Cr, Fe, Mo)_{23}C_6$ after 30 min. A continuous increase in Cr/Fe ratio was also reported with an increase in tempering time at a tempering temperature of 760 ºC. Lower tempering temperature (650 ºC and 700 ºC) has not found a significant effect on dislocation structure and lath morphology of normalized sample. The precipitates evolutions at low tempering temperature were also smaller as compared to tempering at 760 ºC for 1 h of tempering time. Normalizing temperature has also found a great effect on precipitation morphology of fine MX and $M_3X$ precipitates [7]. The precipitates present in the microstructure of P92 steel were dissolved during normalizing treatment, except for MX and $M_3C$. The size of $M_3C$ was reported to be independent of normalizing temperature, while MX size increased with increase in normalizing temperature. The fraction area of both precipitates was observed to decrease with increase in normalizing temperature. Change in chemical composition of MX precipitates was also observed with increase in normalizing temperature. Yoshino et al. [8] also reported that spherical MX and platelet of $M_3C$ were distributed heterogeneously in the normalized condition of P91 steel. The formation of $M_3C$ might have happened during the cooling from normalizing temperature in the lean region of V and Nb in the matrix. Noreña et al. [9] had performed the study related to the evolution of minor phases under different normalizing and tempering condition. In tempering temperature range of 300–400 ºC, the microstructure of P91 steel mainly consisted of Nb-rich spherical shape MX particles, which were not dissolved during normalizing. The evolution of V-rich MX precipitates was observed for tempering above 600 ºC. The size of V-rich MX precipitates was smaller compared to Nb-rich MX. The Fe-rich $M_3C$ precipitates were not dissolved completely during normalizing temperature up to 1250 ºC. $M_3C$ particles were observed at tempering temperature of 500 ºC or below than 500 ºC. Microstructure in furnace-cooled condition that has ferrite and precipitates showed the lower value of diffusion coefficient compared to the air-cooled condition. The minimum value of diffusion coefficient was measured for sample tempered at 500 ºC. The ductile-brittle transition temperature (DBTT) of P91 steel was studied for varying reheat temperature [10]. The strength of P91 steel was observed to increase with an increase in reheat temperature due to the dissolution of existing precipitates in the temperature range of 1025–1100 ºC. The DBTT was observed to be strongly dependent on grain size and higher DBTT was reported for coarse grain structure. Optimum strength and Charpy toughness combination were observed at a normalizing temperature of 1025 ºC. Karthikeyan et al. [11] have also studied the effect of double normalizing treatment on microstructure evolu-

tion, DBTT, creep strength and tensile properties of P91 steel. The double austenitizing based on normalizing and tempering treatment (DNT) was observed to be superior in terms of grain size, tensile properties, creep strength and DBTT characteristic compared to conventional normalizing and tempering treatment (CNT). Long-term ageing was also reported at 550 ºC for 5000 h. The $M_2X$ formation was observed more frequently during long-term exposure for CNT. Laves phase formation was also reported for long-term treatment. Karthikeyan et al. [12] have also reported the similar results for DNT treatment.

Effect of long-term ageing on precipitate evolution behavior and room temperature tensile properties of P92 steel were also performed by many researchers. Homolova´ et al. [13] studied the thermal deformation history on microstructure evolution and stability of P92 steel in the temperature range of 580–650 ºC. For low-temperature range (580–620 ºC), Laves phase formed after the long duration, while for the sample without deformation Laves phase formed after 1000 h of annealing at 650 ºC. For all temperatures, Cr/Fe ratio in $M_{23}C_6$ increased with ageing time. Kafexihu et al. [14] performed ageing of P91 and X20CrMoV121 steel at 650 ºC and 760 ºC for varying ageing time (2 h, 4320 h, 8760 h and 1752 h). The study related to room temperature tensile properties and hardness after long-term ageing was performed. It was observed that tempering at 650 ºC has a relatively small effect on mechanical properties as compared to tempering at 760 ºC. Senior et al. [15] studied the effect of ageing on plastic behavior of 9Cr-1Mo steel. A continuous reduction in ductility was observed with increase in ageing time. The ductility failure was mainly led by inclusion and precipitation of nucleated voids. The reduction in ductility after 1000 h was attributed to nucleation of voids on carbide particles. After 5000 h, Laves phase formation that provided void nucleation sites and led to a reduction in ductility was observed. After Laves phase formation, void nucleation rate at carbides was decreased. Sathyanarayanan et al. [16] have studied the effect of ageing temperature and time on DBTT of P92 steel by using the reference temperature approach under dynamic loading condition ($T_o^{dy}$). At 650 ºC, a drastic increase in $T_o^{dy}$ was observed, while at 600 ºC, a moderate increase was observed. Ageing in the temperature range of 600–650 ºC for 10000 h resulted in the formation of Laves phase that led to embrittling effect and ultimate increase in $T_o^{dy}$. Golañski and Kepa [17] performed the ageing of cast P92 steel and studied its effect on microstructure evolution and mechanical properties. The ageing was performed in the temperature range of 550–600 ºC for varying ageing time (2000 h and 6000 h). Ageing up to 6000 h has a negligible effect on the tensile properties, hardness and lath morphology of P92 steel. Ageing resulted in a drastic decrease in Charpy toughness value. The decrease in Charpy toughness value was attributed to the formation of Laves phase after long-term ageing of 6000 h.

## 2 Materials and methods

The present section has been divided into three parts. The first part deals with the introduction of the "as-received" P92 steel microstructure and mechanical properties. The effect of varying normalizing temperature (950–1150 ºC) on microstructure evolution and mechanical properties of P92 steel has been performed. The tempering is carried out for a fixed temperature of 760 ºC for 2 h. In the second section, the effect of varying tempering temperature and time on the microstructure evolution and mechanical properties has been carried out. The microstructure and mechanical properties have also been studied in the different cooling medium. The third section deals with the evolution of microstructure and degradation of mechanical properties as a result of the long-term ageing.

The base metal used for the experiment was modified 9Cr-1Mo steel (P92) with an outer diameter of 60.3 mm and thickness of 11 mm. P92 steel, also known as modified 9Cr-1Mo-V-Nb steel, is designated as P92 for pipe, T92 for tube and ASTM A335 for the plate. The material in "as-received" condition, according to the manufacturer, was austenitized at 1040 ºC for 10 min and air-cooled, then tempered at 760 ºC for 2 h, and finally air-cooled. The chemical composition of the P92 steel used in the present investigation was evaluated through an optical emission spectrometer (Make: Metavision, model: 1008i) in the laboratory. Chemical composition is depicted in Table 1.

***Table 1. Chemical composition of P92 steel (wt. %)***

| Element | Chemical composition (wt. %) | | | | | | | | | | |
|---|---|---|---|---|---|---|---|---|---|---|---|
| | C | Mn | Cr | Si | Mo | V | Nb | Ni | Ti | Cu | Fe |
| P92 steel | 0.12 | 0.54 | 8.48 | 0.28 | 0.95 | 0.18 | 0.05 | 0.35 | 0.012 | 0.06 | Rest |

The as-received P92 steel was subjected to different heat treatment as discussed below.

The as-received P92 steel was subjected to varying normalizing condition in the temperature range of 950–1150 ºC with a fixed tempering temperature of 760 ºC. The normalizing and tempering conditions are depicted in Table 2. The normalizing was carried out for 60 min.

After the normalizing, P92 steel was subjected to different tempering temperature in the temperature range of 350-1000 ºC for 2 h, and finally air-cooled. The effect of the cooling medium was also studied. The heat treatment matrix for tempering is shown in Table 3.

***Table 2. Conventional normalizing and tempering condition for various samples***

| Sample no. | Normalizing temperature, ºC | Tempering temperature, ºC |
|---|---|---|
| 1 | 950 | 760 |
| 2 | 1000 | 760 |
| 3 | 1050 | 760 |
| 4 | 1100 | 760 |
| 5 | 1150 | 760 |

***Table 3. Different heat treatment regimes performed on P92 steel, investigated in present study***

| Material state | Microstructure | Heat treatment |
|---|---|---|
| as received (AR) | tempered martensite | austenitizing at 1040 ºC for 10 min, air-cooled + tempered at 760 ºC for 2 h |
| air-cooled (AC) | as quenched martensite | AR + austenitizing at 1040 ºC for 40 min, air cooling |
| tempered at 350 ºC and air-cooled (T350-AC) | tempered martensite (partially) | AC + tempered at 350 ºC for 2 h |
| tempered at 650 ºC and air-cooled (T650-AC) | fully tempered martensite | AC + tempered at 650 ºC for 2 h |
| tempered at 760 ºC for 2 h and air-cooled (T760-2-AC) | fully tempered martensite | AC + tempered at 760 ºC for 2 h |
| re-austenitized at 1000 ºC and air-cooled (r-A1000-AC) | as quenched martensite | AC + tempered at 1000 ºC for 2 h |
| tempered at 760 ºC for 2 h and furnace-cooled (T760-2-FC) | fully tempered martensite + ferrite | AC + annealed at 760 ºC for 2 h, furnace-cooled |
| tempered at 760 ºC for 4 h and air-cooled (T760-4-AC) | fully tempered martensite | AC + tempered at 760 ºC for 4 h |
| tempered at 760 ºC for 6 h and air-cooled (T760-6-AC) | fully tempered martensite | AC + tempered at 760 ºC for 6 h |
| tempered at 760 ºC for 8 h and air-cooled (T760-8-AC) | fully tempered martensite | AC + tempered at 760 ºC for 8 h |
| tempered at 760 ºC for 2 h and water-quenched (T760-2-WQ) | tempered martensite | AC + quenched at 760 ºC for 2 h |

In order to reveal the microstructure of heat-treated samples in the different metallurgical state, the metallographic techniques were used. The specimens were polished by emery paper up to grit size of 1500 and the cloth polished using alumina powder. After polishing samples were etched by using Vilella's reagent solution 1 g picric acid + 5 ml HCl + 100 ml ethanol). To characterize the microstructure of heat-treated samples at different magnification SEMQUANTA 200 field emission scanning electron microscope (FESEM) with energy dispersive X-ray spectroscopy (EDS) was used with accelerating voltage of 20 kV, 10-nA probe current for a working distance of 8 mm. The samples used for SEM have also been used for an optical microscope (OM). For phase determination in various heat treatment conditions, X-ray diffraction (XRD) analysis was carried out by using the D-8 Bruker AXS diffract to meter. XRD analysis was performed by using Cu-target, with the working voltage and current of 40 kV and 30 mA, respectively.

The harnesses of P92 steel in as-received and at different heat-treated conditions were measured by using Vicker's micro hardness tester (Omnitech-S Auto) using load value of 500 g and dwell time of 10 s. Static-tensile test at room temperature was performed for both as-received and heat-treated P92 steel as per ASTM A370-14 [18] standard, for gauge length and width of 25 mm and 6.25 mm, respectively. For room temperature tensile tests, Instron 5982 Vertical Tensile Testing was used for constant cross-head speed of 1 mm/min. To study the Charpy toughness of P92 base metal in as-received and heat-treated conditions, standard sub-size V-notch specimens ($55\times10\times7.5$ mm$^3$) were prepared according to ASTM A370-14 [18]. For each test, three samples were prepared and an average of three test results was reported. To study the fracture surface morphology of tensile tested specimen, FESEM analysis was performed.

## 3 Results and discussion

### *3.1 As-received material*

Typical secondary electron, back-scattered and optical micrographs of P92 steel are shown in Fig. 1, a–d. The material was supplied in normalizing and tempering condition. Normalizing of P92 steel results in the formation of martensitic microstructure with high dislocation density with the evolution of precipitates during tempering of steel. The microstructure reveals the presence of the tempered martensitic structure. In the tempered martensitic microstructure, prior austenite grain boundaries (PAGBs) and lath packet / block boundaries are beautified by the coarse carbide precipitates of different shape and sizes. The PAGBs are clearly indicated by the black-dotted line in SEM micrograph as shown in Fig. 1, a. At higher magnification, i.e. 50.0 Kx, accumulation of coarse carbide particles along the PAGBs is clearly observed in Fig. 1, c. The higher density of precipitates along the PAGBs and lower density inside the intra-lath region are also confirmed from the Fig. 1, b. The precipitates decorated along the PAGBs and lath boundaries were confirmed as Cr, Fe and Mo-rich $M_{23}C_6$, while inside the intra-lath region they were confirmed as V and Nb-rich MX(X: C, N) [9, 19]. It is difficult to observe the fine MX precipitates because of very small size in the order of 15–40 nm [20]. Higher Cr concentration at the PAGBs and higher carbon diffusion coefficient are mainly responsible for the formation of Cr-rich $M_{23}C_6$ type precipitates. In as-received condition (N&T) of P92 steel, 70% of MX type precipitates belong to V(C&N) and remaining 30% – to Nb (C&N). The primary Nb-rich MX type precipitates form during the normalizing, while secondary MX precipitates (mainly VN) form during the tempering treatment. The optical micrograph shows the presence of PAGBs, sub-grain boundaries and precipitates, as shown in Fig. 1, d. Inside the sub-grain boundaries, high dislocation density was reported by Panait et al. [20]. The average grain size measured for as-received P92 steel from SEM micrograph was about 35±12.54 μm and good agreement was found with grain size measured from the optical micrograph of as-received base metal, which was about 41±10.45 μm. The grain size was observed to be similar as reported by Arivazhagan and Kamraj [21].

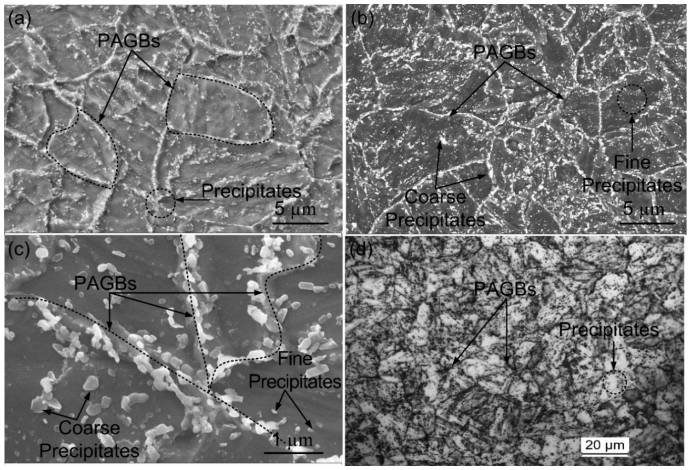


***Fig. 1. Typical secondary electron micrograph of P92 steel (a); backscattered electron image (b); secondary electron micrograph at 50Kx showing $M_{23}C_6$ coarse precipitates at grain boundary and fine $M_{23}C_6$ and MX precipitates in the inter-lath region (c); typical optical micrographs (d)***

The energy dispersive X-ray spectroscopy (EDS) was carried out to identify the precipitates present along the PAGBs and grain interior region. Table 4 shows the chemical composition of marked location in Fig. 2. From Table 4, coarse precipitate at the point A (PAGBs) is identified as Cr, Fe and Mo-rich $M_{23}C_6$. The point B shows higher Nb concentration of 4.97 wt% and 0.62 wt% V, which indicates the formation of V and Nb-rich MX particles. 7.32 wt% Cr and 0.14 wt% Nb at point D are higher than 6.20 wt% Cr and 0.00 wt% Nb at point C due to the local dissolution of the $M_{23}C_6$ carbide. Point E indicates the chemical composition of Fe-rich matrix region that has 8.78 wt% Cr and 80.78 wt% Fe. The similar results have also been reported by Wang et al. [22].

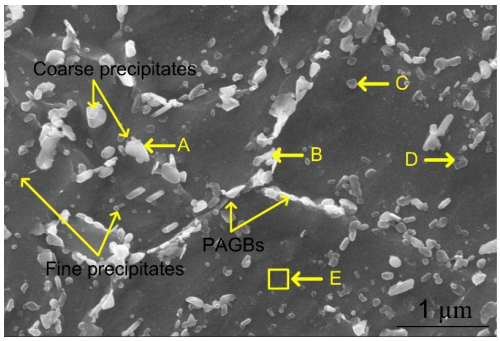


***Fig. 2. Marked location in the microstructure of P92 steel for the EDX point analysis***

The EDS spectra of precipitates (Fig. 3, a) located along the PAGBs is shown in Fig. 3, b. The SEM-EDS analysis of precipitates confirmed the presence of Cr, Fe, Mo and V elements. The presence of secondary phase elements confirms the formation of $M_{23}C_6$ phase (M: Cr, Fe, and Mo), while V presence indicates the formation of fine VC precipitates. The line elemental mapping of precipitates was also carried out, as shown in Fig. 3, b. The line elemental mapping reveals that higher Cr concentration is encountered in $M_{23}C_6$ phase. The concentration of V and Mo remains the same while Fe concentration goes down. As-received mechanical properties of P92 steel are depicted in Table 5.

***Table 4. Chemical composition of Point A to E marked in Fig. 2***

| Points | Points Element composition (wt%) | | | | | | | Possible phase |
|---|---|---|---|---|---|---|---|---|
| | Fe | Cr | Mo | Si | Mn | V | Nb | |
| A | 69.11 | 14.60 | 2.32 | 0.51 | 0.45 | 0.20 | 0.16 | Cr-Mo-rich $M_{23}C_6$ |
| B | 66.30 | 10.03 | 1.43 | 0.46 | 0.09 | 0.62 | 4.97 | V-Nb rich MX |
| C | 69.16 | 6.20 | 0.83 | 0.42 | 0.41 | 0.33 | - | Fe-rich matrix |
| D | 65.78 | 7.32 | 1.08 | 0.45 | 0.25 | 0.05 | 0.14 | Fe-rich matrix |
| E | 80.84 | 8.78 | 1.23 | 0.51 | 0.68 | 0.09 | 0.37 | Fe-rich matrix |

***Table 5. Mechanical properties of P92 steel in as-received state***

| P92 steel | Yield strength, MPa | Tensile strength, MPa | Elongation, % | Hardness, HV | Toughness, J |
|---|---|---|---|---|---|
| | 475±25 | 715±15 | 20±2 | 247±5 | 198±8 |

The XRD pattern for P92 steel in the as-received state is shown in Fig. 4. P92 steel might contain the following precipitates: carbides or carbonitride $M_3C$, M(C, N), $M_2$(C, N), $M_7C_3$, $M_{23}C_6$ (M stands for metallic solute atom such as Fe, Cr, Mn, V, Nb, Mo) and other inter metallic precipitates. The sequence of precipitation for P92 steel is as follows [23]:

$$M_3C + MC \rightarrow M_3C + MC + M_{23}C_6 \rightarrow M_3C + MC + M_{23}C_6 + M_7C_3 \rightarrow MC + M_{23}C_6 + M_7C_3. \quad (4)$$

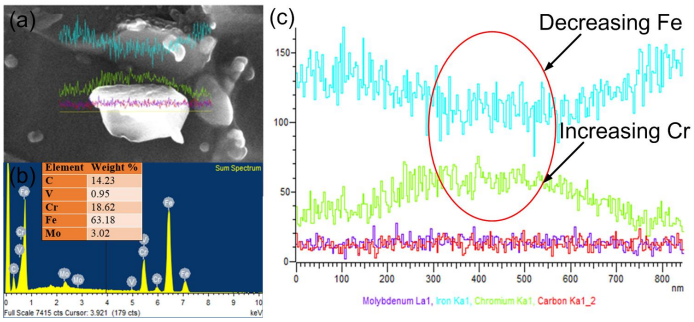


***Fig. 3. Precipitate selection showing for:***
a – line mapping; b – EDS spectra of white $M_{23}C_6$ particle;
c – line mapping of white $M_{23}C_6$ particle

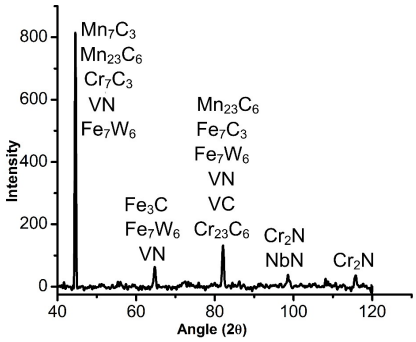


***Fig.4. X-ray diffraction pattern for "as-received" P92 steel***

***Table 6. Structure and lattice parameter of phases identified in XRD analysis***

| S. no | Phase identified | Structure | Lattice parameter (A°) | Density (gm/cm$^3$) |
|---|---|---|---|---|
| 1 | $Cr_{23}C_6$ | Cubic | a=10.63, b=10.63, c=10.63 | 6.97 |
| 2 | $Mn_{23}C_6$ | Cubic | a=10.58, b=10.58, c=10.58 | 7.48 |
| 3 | $Cr_7C_3$ | Orthorhombic | a=7.01, b=12.15, c=4.53 | – |
| 4 | $Mn_7C_3$ | Orthorhombic | a=6.94, b=11.98, c=4.54 | 7.39 |
| 5 | $Fe_7C_3$ | Hexagonal | a=6.88, b=6.88, c=4.54 | 7.61 |
| 6 | $Fe_3C$ | Orthorhombic | a=5.04, b=6.73, c=4.51 | 7.80 |
| 7 | $Cr_2N$ | Cubic | a=4.81, b=4.81, c=4.81 | 6.78 |
| 8 | VC | Cubic | a=4.165, b=4.165, c=4.165 | 5.64 |
| 9 | VN | Cubic | a=4.09, b=4.09, c=4.09 | 6.30 |
| 10 | NbC | Cubic | a=4.47, b=4.47, c=4.47 | – |
| 11 | NbN | Cubic | a=4.92, b=4.92, c=4.92 | 8.35 |

Through the XRD pattern, the phase identified in the as-received state of P92 steel are Mn and Cr-rich $M_{23}C_6$, Nb-rich MX particles, Fe, Cr and Mn-rich $M_7C_3$, and Cr-rich $M_2X$. Structure and lattice parameter obtained for each phase are represented in Table 6. The similar lattice parameter and structure for MX and $M_{23}C_6$ phase was also reported by Huntao-Norena et al. [24].

### *3.2 Effect of normalizing temperature*

#### *3.2.1 Microstructure evolution*

Microstructures of P92 steel for different normalizing conditions (Table 2) are shown in Fig. 5, a–b. Normalized steel mainly exhibits lath martensitic structure with distinct PAGBs. The martensitic laths have a spatial orientation in one direction within lath packets or groups inside the prior austenite grains (PAGs), as shown in Fig. 5, b. Normalizing results in dissolution of $M_{23}C_6$ and V-rich MX precipitates. P92 steel has very high tendency to form martensite even under slower cooling rate, i.e. furnace cooling. For a higher normalizing temperature of 1150 ºC, dissolution of precipitates and width of lath boundary are found to be increased, as shown in Fig. 5, b. Yoshino et al. [7] also reported the decrease in fraction area of precipitates with an increase in normalizing temperature. The undissolved precipitates are clearly seen in higher magnification micrograph, as shown in Fig. 5, c. It was reported that the precipitates which remain undissolved during the normalizing are mainly MX and Fe-rich $M_3C$. The presence of MX and Fe-rich $M_3C$ particles after normalizing in the temperature range of 600–1240 ºC was also reported by Jones et al. [6].

Maruyama et al. [25] reported that the precipitate that remains undissolved is mainly Type I NbX. Size of undissolved spherical particles is observed to be varied from 30 to 90 nm. Length of platelets shape elongated particles is varied 80 to 120 nm and width is varied from 15 to 25 nm. Spherical shape particles were confirmed as Nb-rich MX while platelets shape as $M_3C$ [24]. EDS spectra of EDS spot 1 and EDS spot 2 confirm that the particles present in the matrix and lying along the lath boundaries are mainly Cr, Fe, Mo and Nb. The higher weight percentage of Fe and C confirms the presence of $Fe_3C$, while Nb indicates the presence of NbC precipitates.

Tempering of normalized P92 steel resulted in the formation of tempered martensite with the evolution of precipitates that provide the stability to microstructure. The micrographs of P92 steel in different normalizing and tempering (N&T) conditions are shown in Fig. 6.

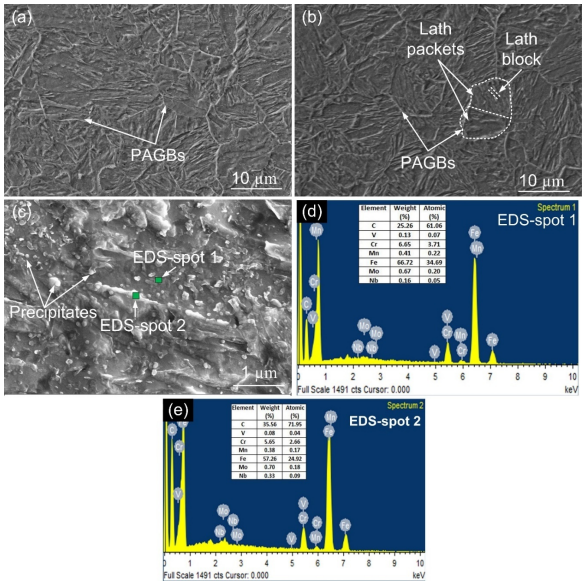


***Fig. 5. Secondary electron micrograph of P92 steel normalized at (a–c )higher magnification micrograph of steel normalized at showing un-dissolved precipitates and EDS spectra of EDS(within grain(d, e) EDS spectra of EDS (at the grain boundary) showing:***
a – 950 ºC; b – 1150 ºC ; c – 950 ºC; d – spot 1; e –spot 2

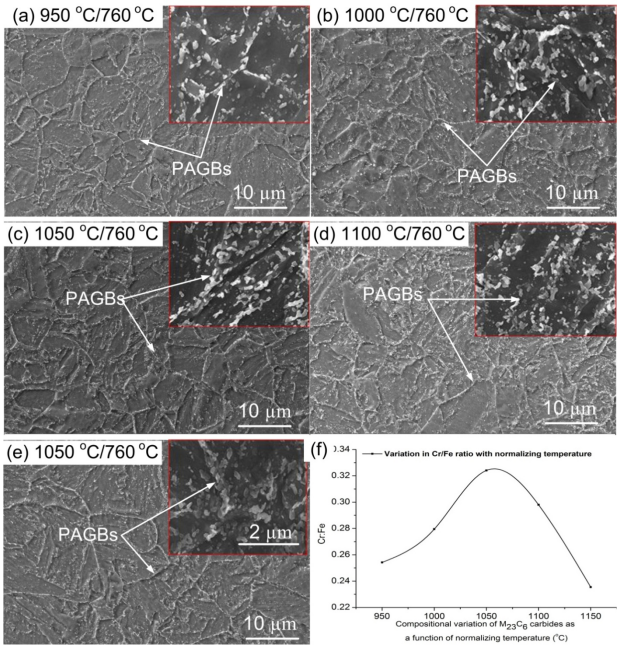


***Fig. 6. SEM micrograph of P92 steel in normalizing and tempering conditions (a–e) and compositional variations of $M_{23}C_6$ carbides as a function of normalizing temperature (f):***
a – 950 ºC/760 ºC; b – 1000 ºC/760 ºC; c – 1050 ºC/760 ºC; d –1100 ºC/760 ºC ; e – 1150 ºC/760 ºC

Tempering was performed at a constant temperature of 760 ºC for 2 h. SEM micrograph at higher magnification, i.e. 50.0 Kx, is shown in the top right corner of respective low magnification micrographs. SEM micrograph at higher magnification is used in the further study of particles distribution and their size measurement. The higher density of coarse particles having different size and shape is observed along the PAGBs, sub-grain boundaries, and lath blocks. The intra-lath region shows the uniform distribution of fine spherical precipitates. The coarse precipitates located along the boundaries are confirmed as Fe, Cr and Mo-rich $M_{23}C_6$, while inside the intra-lath region those are V and Nb-rich MX [20, 22]. For a fixed tempering temperature, increase in normalizing temperature leads to a reduction in the availability of grain boundaries for the precipitation to occur, which might be the cause of the decrease in area fraction of precipitates. After N&T, heterogeneity in size of precipitates was noticed. The size of precipitates was observed to be varied from 35 nm to 240 nm. For a fixed tempering temperature of 760 ºC, the relative change in the composition of $M_{23}C_6$ carbide with normalizing temperature is shown in Fig. 6, f. The various elements present in $M_{23}C_6$ carbides and their ratio was quantified from the EDS spectra. For base metal, Cr/Fe ratio was calculated and is about 0.295. A continuous increase in the Cr/Fe ratio with normalizing temperature was observed up to a normalizing temperature of 1050 ºC and after that, it decreased. The minimum and maximum value of Cr/Fe ratio were calculated for a normalizing temperature of 1150 ºC and 1050 ºC, respectively. The increase in Cr/Fe ratio is attributed to the evolution of meta stable $M_{23}C_6$ phase due to thermal activation that drives diffusion of Cr into the carbides and $M_{23}C_6$ progresses towards achieving the thermally stable $Cr_{23}C_6$ configuration [26].

The schematic evolution of precipitates and lath boundaries, lath packets and lath blocks during the normalizing and tempering process is shown in Fig. 7.

In the as-received state, size of precipitates was observed to be varying from 25 to 285 nm. The precipitates having a size in the range of 20 to 40 nm are confirmed as MX precipitates [20]. The average size of carbide precipitates present at the grain boundary and intra-lath was observed to be 194±25 nm and 135±20 nm, respectively. The average precipitate size was measured to be 145±40 nm. A comparative study of the size of particles present at the grain boundary and within the grain in different N&T conditions is given in Fig. 8, a–b.

From Fig. 8, a–b, it was observed that with an increase in normalizing temperature, size of precipitates present at the PAGBs and within matrix decreased up to a normalizing temperature of 1100 ºC, beyond that a drastic increase was observed, which is quite harmful from creep strength point of view. The $M_{23}C_6$ particles are more effective in enhancing the creep life of P91 steel compared to other carbide precipitates as the size of carbide particles is similar to the thickness of "sub-grains" boundaries, which makes it difficult for sub-grain to cross the carbide precipitates $M_{23}C_6$ during creep. Hence, $M_{23}C_6$ carbide particles provide most effective pinning at sub-grain boundaries and enhance creep strength by preventing dislocation. The carbide particles $M_{23}C_6$ in the range of 100–200 nm were observed to be more effective in pinning the grain boundaries [27]. Normalizing beyond 1150 ºC resulted in a drastic increase in the size of precipitates, however, it was less than the particle size of the as-received material. Hence, normalizing of P91 steel beyond 1150 ºC was not preferable.

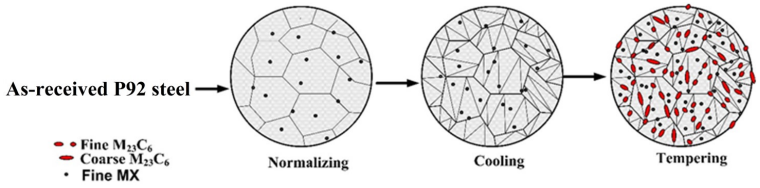


***Fig. 7. Schematic evolutions of precipitates during normalizing and tempering***

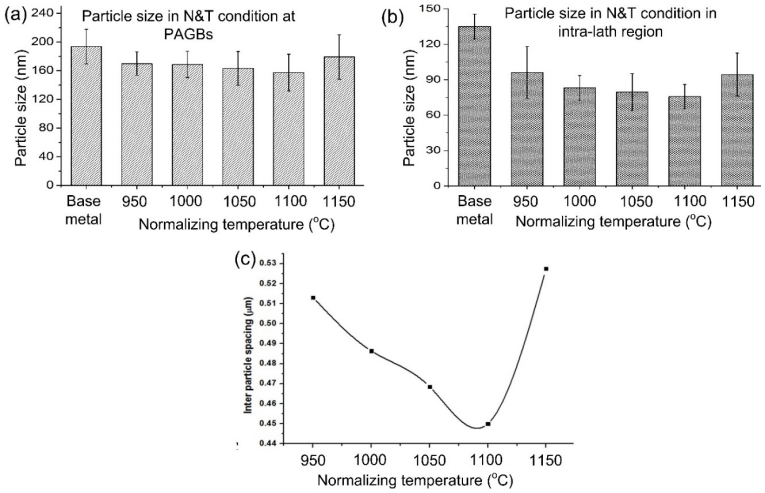


***Fig. 8. Variation in particle size for varying normalizing and fixed tempering temperature at (a, b) region and variation in particle-to-particle distance for varying N&T condition (c):*** a – PAGBs; b – inside intra-lath

The average particle-to-particle distance mainly depends upon carbide phase (f) and size of particles (d). The particle-to-particle spacing (L) is given by equation (4) [28]

$$l = \frac{4d}{\pi f^{\frac{1}{3}}}. \quad (5)$$

For the same quantity of carbide phase, the introduction of data relevant to the P91 tested steel in equation (5) gives $L$=3.86$d$. According to this, particle-to-particle distance grows four times faster than particle size.

The inter-particle spacing is graphically presented in Fig. 8, c. For constant tempering temperature, increase in normalizing temperature results in a reduction in inter-particle spacing and it continues up to 1100 ºC and after that increases drastically up to 0.53 μm.

Optical micrograph of P92 steel in different N&T conditions is shown in Fig. 9, a–c. Tempering of normalized P92 steel results in carbon and nitrogen rejection from solid solution and formation of carbide and nitride precipitates. Sub-grain boundaries are observed inside the prior-austenite grains (PAGs).The precipitates along the PAGBs, sub-grain boundaries, lath boundaries and inside the matrix region are clearly seen in the optical micrograph. From Fig. 9, d, it is clearly seen that for fixed tempering temperature, increase in normalizing temperature leads to the grain coarsening. For P92 steel normalized at 1150 ºC when it undergoes tempering process, a great amount of coarsening observed, as shown in Fig. 9, d. For N&T P92 steel, small variation was observed in grain size up to a normalizing temperature of 1100 ºC and after that drastic increase was observed as a result of dissolution of precipitates, as shown in Fig. 9, d.

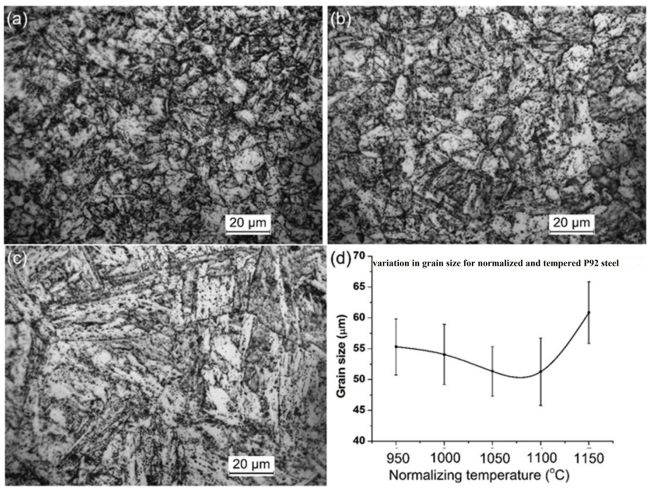


***Fig. 9. Optical micrograph of P92 steel for different N&T condition (a–c) and variation in grain size for different normalizing temperature (ºC) and fixed tempering temperature (760 ºC) (d):*** a – 950 ºC/760 ºC; b – 1050 ºC/760 ºC; c – 1150 ºC/760 ºC

### *3.2.2 Tensile properties*

For a fixed tempering temperature, variation in ultimate tensile strength (UTS) and yield strength (YS) value with normalizing temperature is shown in Fig. 10, a–b. YS and UTS are observed to be increased with increase in normalizing temperature. Initially, with a change in normalizing temperature from 950 ºC to 1000 ºC, changes in UTS and YS are very high. After 1000 ºC, with an increase in normalizing temperature, the rate of change in UTS was found to be very small and degree of change in YS was almost constant.

The steel normalized at a higher temperature, i.e. 1150 ºC, shows high YS and UTS because of coarse grain size and lath width. Coarse grain structure results in smaller availability of grain

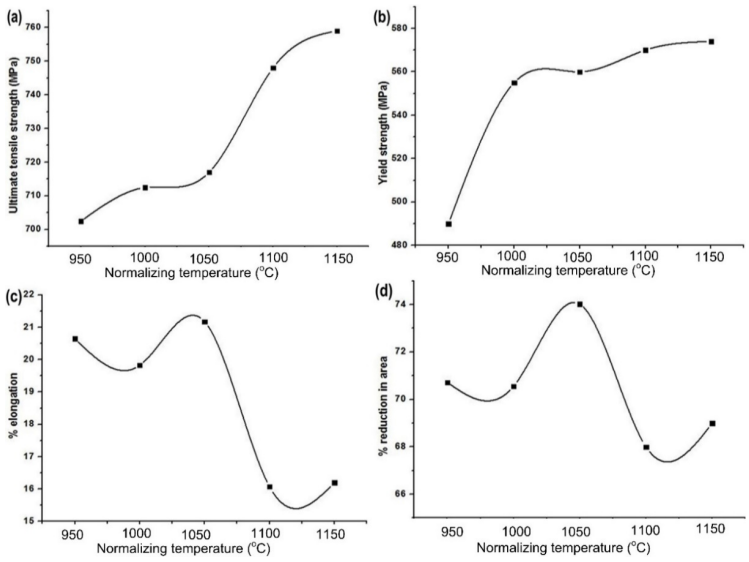


***Fig. 10. Variation in ultimate tensile strength showing:*** a – yield strength; b – % elongation; c – % reduction in area; d – with N&T conditions

boundaries per unit area that leads to the smaller precipitation of carbides and carbonitrides and ultimately higher availability of carbon (C) and nitrogen (N) in the solution matrix. The higher availability of C and N in the solution matrix leads the solid solution strengthening that results in increases in UTS and YS of sample normalized at 1150 ºC compared to other samples normalized in the temperature range of 950–1100 ºC. The percentage elongation and percentage reduction in the area for varying normalizing temperature are shown in Fig. 10, c–d. Both are observed to be decreased with increase in normalizing time from 950 ºC to 1000 ºC for constant tempering time and then increased from 1000 ºC to 1050 ºC and beyond that decreased continuously up to 1150 ºC.

### *3.2.3 Hardness and Charpy toughness*

The hardness of P92 steel was measured to be 247±5 HV in the as-received state as given in Table 5. Microhardness of P92 steel in different normalizing and N&T conditions are shown in Fig. 11, a–b. The hardness of P91 steel depends on various terms such as the fine MX precipitates, grain size, dislocation density, precipitation hardening, and solid solution strengthening [29, 30]. The microhardness of P92 steel was observed to be increased with increase in normalizing temperature and it might be due to increase in the quantity of fresh martensite, and solid solution hardening. The fraction area of MX and $M_3C$ was reported to be decreased with increase in normalizing temperature [7]. The dissolution of precipitates with an increase in normalizing temperature leads to solid solution strengthening due to higher availability of C and N in the solution matrix. This might be one of the possible causes of the increase in hardness of P92 steel with an increase in normalizing temperature. During tempering treatment of these normalized samples for given tempering temperature of 760 ºC, the hardness decreased due to the tempering of martensite and reduction in solid solution hardening. Tempering process results in the evolution of precipitates that leads to precipitation hardening but at the same time reduction in C and N in the solution matrix leads to the reduction in solid solution hardening. The reduction in solid solution hardening dominates over the increase in precipitation hardening that results in a reduction in hardness value after the tempering process. For constant tempering temperature, microhardness was observed to be increased with increase in normalizing temperature, as shown in Fig. 11, b. However, the degree of hardness, which increased for the samples normalized in the temperature range of 950–1000 ºC and 1050–1100 ºC, was found to be relatively lower compared to the degree of increase in hardness for samples normalized in the temperature range of 1100–1150 ºC. Sample normalized at low temperature shows fine grain structures, coarsening of undissolved precipitates, and precipitation of large number of carbides (solution becomes depleted from C and N) during tempering, which might be the cause of lower hardness. However, in case of high normalizing temperature, tempering results in lower precipitation of carbides due to smaller availability of precipitate nucleation sites (PAGBs, lath boundaries). A large number of C and N present in solid solution leads to the solid solution strengthening that results in higher hardness value at higher normalizing temperature.

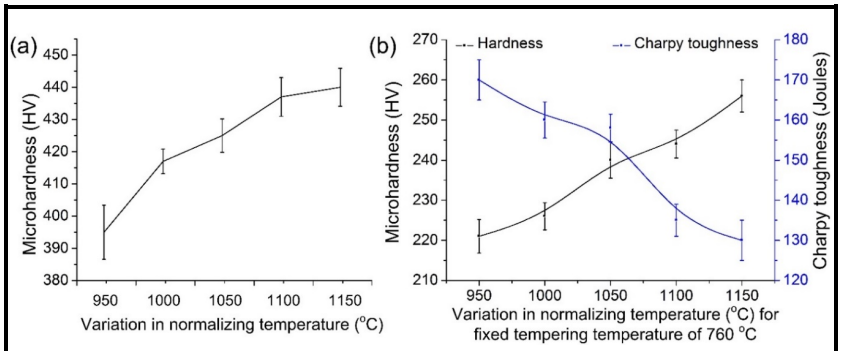


***Fig. 11. Variation of hardness with normalizing temperature showing:***
a – variation in hardness and Charpy toughness; b – for varying N&T conditions

In an as-received state, the room temperature Charpy toughness of base metal was measured to be about 198±8 Joules. At constant tempering temperature of 760 ºC, variation in room temperature Charpy toughness of P92 steel with normalizing temperature is shown in Fig. 11, b. The Charpy toughness was observed to be decreased with the increase in normalizing temperature. It was also observed that the extent of reduction in toughness with an increase in normalizing temperature was uniform up to 1050 ºC. However, a drastic reduction in toughness (about 15%) was observed with increase in normalizing temperature from 1050 ºC to 1100 ºC. With higher normalizing temperature, the cracking of secondary particles and decohesion at the precipitate/matrix occurred, which in turn resulted in reduction in toughness of P92 steel. Higher solid solution hardening also results in the formation of brittle columnar lath martensite with higher C percentage that leads to poor toughness for higher normalizing and constant tempering temperature.

### *3.3 Effect of tempering temperatures and cooling conditions*

After the study of varying normalizing temperature, the study of the effect of varying tempering temperature on microstructure evolution and mechanical properties of P92 steel for a fixed normalizing temperature was performed. For further study on the effect of tempering temperature on microstructure evolution and mechanical properties of P92 steel, normalizing was carried out at 1040 ºC for 40 min, followed by air cooling.

#### *3.3.1 Effect of tempering temperatures and cooling conditions*

Secondary electron micrograph in AC (normalized) condition for different magnification is shown in Fig. 12. Low magnification micrograph shows untempered lath martensite in form of packets or groups within PAGBs and sub-grain boundaries. At low magnification, negligible precipitates were observed along the boundaries and inside the intra-lath region, as shown in Fig. 12, a. The spatial orientation of martensitic lath present within prior austenite grain boundaries and heterogeneous distribution of undissolved precipitates are clearly shown in Fig. 12, b. The length of the packets or groups varies from 5.43 to 15 μm and width varies from 3.52 to 8.5 μm. The average grain size was measured to be 50±16 μm. The undissolved precipitates are confirmed as spherical MX and coarse platelet of $M_3C$ cementite [24]. Jones et al. [6] have also reported the presence of NbC and $(Fe, Cr)_3C$ as undissolved precipitates in P92 steel after the normalizing. The formation of $M_3C$ might happen during the cooling from normalizing temperature in the lean region of V and Nb in the matrix. The particles inside the intra-lath region show spherical shape. The size of precipitates is measured in the range of 50–169 nm, except for a single particle of size 230 nm. The average precipitate size is measured as 85±35 nm, which is higher than the size of spherical precipitates measured after normalizing at 950 ºC. A few particles with size less than 40 nm were also observed.

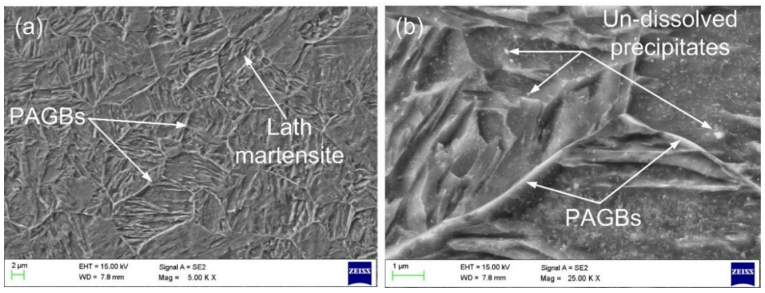


***Fig. 12. SEM micrograph of P92 steel in AC condition showing:*** a – PAGBs and lath martensite, b – undissolved precipitates

***Table 7. Mechanical properties of P92 steel in normalized state (AC)***

| P92 steel | Yield strength, MPa | Tensile strength, MPa | Elongation, % | Hardness, HV | Toughness, J |
|---|---|---|---|---|---|
| | 900±20 | 1363±15 | 16±1.5 | 461±8.54 | 68±4 |

The particle with the size less than 30 nm was difficult to resolve using the SEM. The coarsening of undissolved precipitates with an increase in normalizing temperature was also reported by Yoshino et al. [8]. Mechanical properties of P92 steel in the normalizing state are given in Table 7. Higher YS, UTS and hardness in AC state are attributed to the presence of untempered brittle martensite in the microstructure.

#### *3.3.2 Tempering effect on microstructure evolution*

After the normalizing, tempering was performed as per Table 2. Initially tempering was performed at 350 ºC for 2 h (T350-AC). In T350-AC condition, secondary electron micrograph in different magnification is shown in Fig. 13, a–b. In T350-AC condition, no significant change was observed in the microstructure as compared to AC condition. Microstructure represents the typical lath martensitic structure, as shown in Fig. 13, a. Lath blocks and undissolved precipitates are shown in Fig. 13, b. Small particles were observed inside the intra-lath region at higher magnification having diverse morphologies and sizes. The size of precipitates was measured in the range of 30–178 nm with an average size of 80±30 nm. The reduction in average precipitate size after tempering at 350 ºC is attributed to the formation of new fine MX precipitates. Cr and Fe-rich $M_7C_3$ particles evolution during

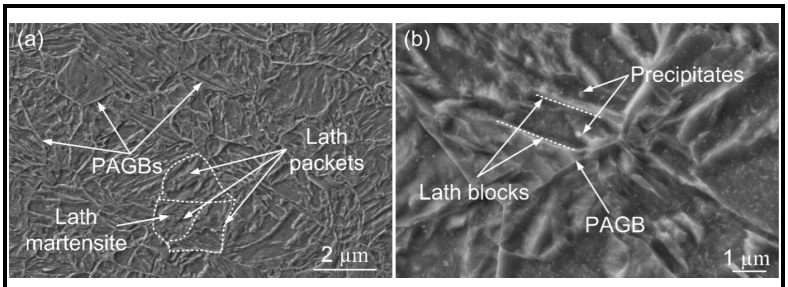


***Fig. 13. Microstructure of P92 steel after tempering at 350 ºC (T350-AC):*** a – in low magnification; b – at high magnification

tempering was also observed [19]. The length of the packets region is varied from 7.34 to 15.26 μm and width is varied from 2.78 to 11.78 μm. The average grain size for T350-AC measured was about 49±15 μm, which is almost similar to AC condition of P92 steel.

The microstructure of P92 steel after tempering at 650 ºC (T650-AC) consists of a higher density of precipitates as compared to T350-AC, as shown in Fig. 14, a. The microstructure mainly consists of tempered martensite with $M_{23}C_6$ and MX precipitates. The decoration of carbide precipitates along the PAGBs and martensitic lath boundaries is clearly observed from Fig. 14, b. The higher density of precipitates along the boundaries is clearly observed in the back-scattered micrograph. In 650-AC condition, precipitates mainly consist of Cr, Fe and Mo-rich $M_{23}C_6$ carbides, Cr-rich $Cr_2C$ and NbX carbonitrides [6]. Size, shape and distribution of particles inside the matrix and along the boundaries are clearly observed in Fig. 14, c. The globular shape and needle shape particles are observed along the PAGBs, while almost spherical shape particles were observed inside the intra-lath region. The particle size is observed to be varied from 30–220 nm with average size about 112±45 nm. The particle having size less than 40 nm is considered as V and Nb-rich MX precipitates [20]. From SEM micrograph, average grain size measured for the T650-AC condition was about 46±26 μm. Fig. 14, d shows the EDS spectra of white particles present along the PAGBs (Fig. 14, c). The EDS spectra confirm the presence of secondary phase carbide particles. The higher weight percentage of Cr, Fe and Mo confirms the formation of $M_{23}C_6$ precipitates along the PAGBs.

The P92 steel heated at 760 ºC (T760-2-AC) for 2 h shows the formation of fully tempered martensite, as shown in Fig. 15, a. A larger number of $M_{23}C_6$ type carbide precipitates is distributed along PAGBs and lath boundaries. The fine vanadium and niobium rich MX type precipitates are dispersed within grains and strengthen the matrix phase. After tempering at 760 ºC, grain size reduced as compared to steel tempered at 650 ºC that results in the number of grains per unit area

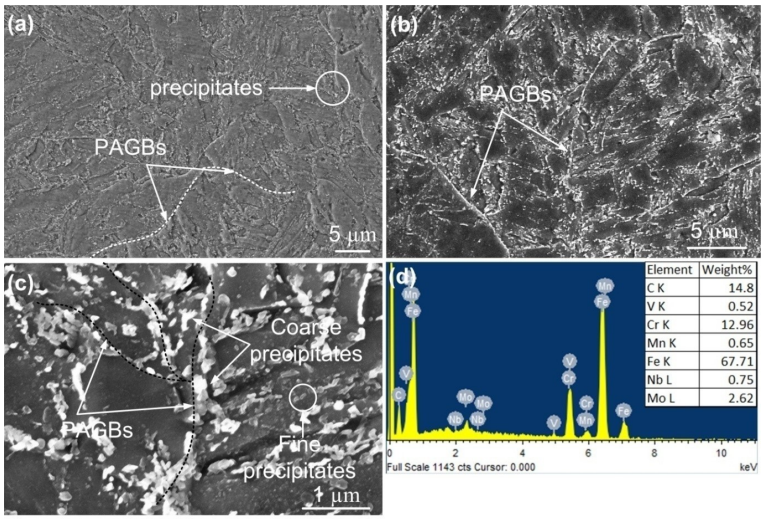


***Fig. 14. Micrograph of P92 steel in T650-AC condition:***
a – secondary electron micrograph; b – back-scattered micrograph;
c – micrograph at higher magnification;
d – EDS spectra of particles located along PAGBs

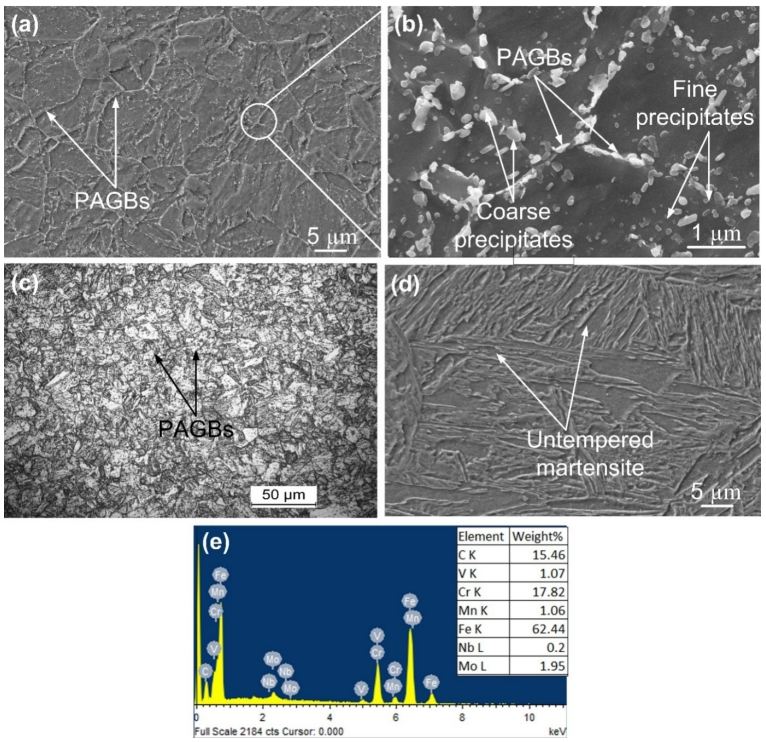


***Fig. 15. Micrograph of P92 steel in T760-2-AC condition:***
a – micrograph at 5000x; b – micrograph at 50000x;
c – optical micrograph at 500x;
d – micrograph for r-A1000-AC condition;
e – EDS spectra of particle for T760-2-AC condition

being increased and provides the sides for large precipitation of carbide particles. Hence, in the T760-2-AC condition, the number of grains, number density of precipitates along sub-grain boundaries and precipitate density within grain increased compared to T650-AC and T350-AC condition. Morphology of precipitates present along the PAGBs and inside the intra-lath region is shown in Fig. 15, b.

The particles sizes were observed to be varied from 31–246 nm with average particle size about 110±39 nm. Hence, no change in the average size of precipitates was observed with increase in tempering temperature from 650 ºC to 760 ºC. The size of prior austenite grains was measured to be about 39±6 μm. A typical optical micrograph is shown in Fig. 15, c. For T650-AC condition, limited $M_{23}C_6$ and MX precipitates were reported as compared to T760-2-AC [15]. In AC condition, the presence of Cr and Fe-rich $M_3C$ precipitates is observed. The tempering at lower temperature results in the formation of Cr-rich $Cr_2C$ phase, which further transformed into $M_{23}C_6$ with the dissolution of $M_3C$ phase.

Tempering at 1000 ºC (r-A1000-AC) for 2 h produced a considerable change in the microstructure as compared to T760-2-AC condition (below $A_{c1}$ temperature), as shown in Fig. 15, d. Tempering at 1000 ºC can be considered as the re-austenitizing of steel. Tempering at 1000 ºC resulted in the dissolution of precipitates that leads the C and N percentage in the solution matrix. That results in the formation of brittle fresh martensite. Length of platelets shape $Fe_3C$ cementite particles varies from 80 to 565 nm and width varies from 80 to 217 nm. The average size of spherical particles was measured to be 90±45 nm, which indicates the coarsening of undissolved precipitates as compared to AC and T350 condition.

### *3.3.3 Furnace-cooled (T760-2-FC) and water-quenched (T760-2-WQ) condition*

Heating at 760 ºC for 2 h with subsequent slow cooling (FC) results in austenite transformation to ferrite, as shown in Fig. 16, a. Furnace cooling results in the non-uniform ferrite grain size with a higher density of coarse carbide precipitates mainly along the PAGBs. Compared to air cooling (T760-2-AC), furnace cooling produced the coarse grains. The microstructure is characterized by the presence of coarse and fine precipitates with equiaxed tempered martensite. After the furnace cooling, carbide precipitates of average size about 158±40 nm were observed, this was much higher than in the T650-AC and T760-2-AC condition. The size of particles was observed to be varied from 35–268 nm. The density of coarse precipitates was observed to be higher as compared to fine precipitates. Coarsening of PAGs is also observed after the furnace cooling. The average grain size measured in T760-2-FC condition was about 51±18 μm from SEM micrograph. A good agreement was found with grain size measured from the optical micrograph, which was about 48.17±16.65 μm. The micrograph of P92 steel in water-quenched (T760-2-WQ) state is shown in Fig. 16, c–d. The typical columnar lath morphology is clearly seen from Fig. 16, c. The accumulation of carbide particles at the lath blocks is clearly indicated in Fig. 16, d. The microstructure mainly consisted of elongated lath martensite with an average width of 0.722±0.143 μm. In higher magnification micrograph, mainly globular and spherical shape coarse particles were observed. The average size of precipitates present both at the lath boundaries and in the matrix was calculated to be 159±47 nm, which was similar to the particle size in the T760-2-FC state. The particles size was observed to be varied from 35–276 nm that indicates the presence of higher density of coarse precipitates. Dislocation density was also observed to be higher in T760-2-WQ condition.

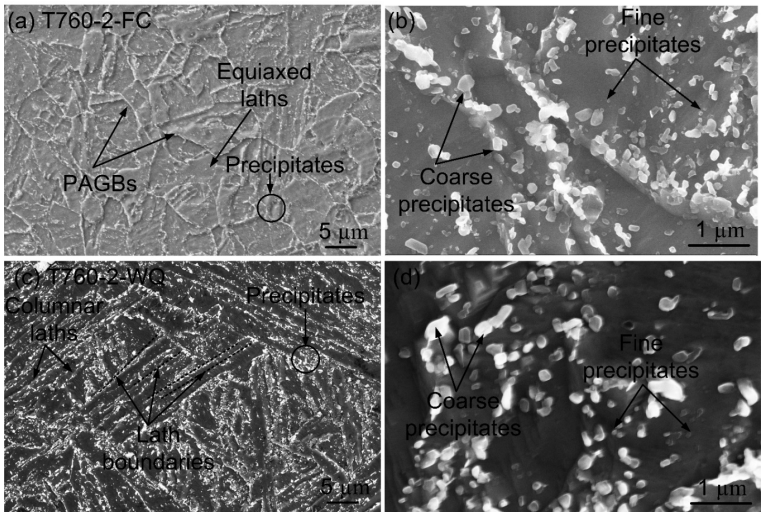


***Fig. 16. Micrograph in furnace-cooled condition (a, b) and in water-quenched condition (c, d) showing:***
a – grain boundaries and precipitates; b – morphology of precipitates; c – lath boundaries and precipitates; d – morphology of precipitates

### *3.3.4 Tensile properties*

Fig. 17, a shows the effect of different tempering temperature on yield strength (YS), and ultimate tensile strength (UTS) of P92 steel. Maximum YS and UTS were measured in AC condition at about 900 MPa and 1363 MPa. Higher UTS and YS in AC condition are attributed to the presence of untempered lath martensite and higher slid solution hardening. YS and UTS decreased after the tempering. Tempering of P92 steel included the lath break up, carbides precipitation, reduction in solid solution hardening due to precipitation, reduction in dislocation density and thermal straining of existing precipitates. Tempering at 350 ºC did not produced any significant effect on YS and UTS as compared to AC state because of ineffective tempering reaction. Increase in tempering temperature from 350 ºC to 650 ºC produced a drastic decrease in the YS and UTS due to the tempering of martensite and evolution of precipitates. Tempering reaction resulted in the higher evolution of C and N from the solution matrix that led to a reduction in solid solution strengthening. This resulted in a reduced value of YS and UTS in T650-AC condition compared to T350-AC conditions. Tempering at 760 ºC resulted in further reduction of YS and UTS of P92 steel. In T650-AC and T760-2-AC, reduction in solid solution hardening dominates to increase in precipitation hardening. Further, re-austenitizing of steel in AC condition increases the YS and UTS compared to the T760-2-AC condition due to the dissolution of precipitates and formation of untempered lath martensite. In r-A1000-AC condition, high solid solution hardening led to higher YS and UTS.

In T760-2-FC condition, lower YS and UTS were observed because of grain and precipitates coarsening. The lower YS and UTS were also obtained in WQ condition as shown in Fig. 17, a. The YS and UTS are strongly affected by the tempering temperature. The increase in tempering temperature below the lower critical temperature leads to decrease in YS and UTS. The decrease in YS and UTS is strongly affected by area fraction of precipitates, their size and size of the grain. The coarser precipitates at higher temperature have fewer tendencies to act as dislocation movement barrier, which may cause the decrease in strength. In r-A1000-AC conditions, due to dissolution of precipitates, C and N came into the solution matrix and aided solid solution hardening. This resulted in enhanced YS and UTS in r-A1000-AC condition.

Percentage elongation for base metal in the as-received state was found to be 20% for gauge length of 25 mm. In AC state, a significant change in elongation and reduction in area were observed because of brittle fracture. Variation in % elongation and reduction in area for the tensile tested specimen with the increase in tempering temperature are shown in Fig. 17, b. The percentage elongation was observed to be increased with increase in tempering temperature from 350 ºC to 760 ºC. The steel tempered at 760 ºC exhibited good ductility along with better YS and UTS. After 760 ºC, there is an increase in tempering temperature, i.e. r-A1000-AC state. A drastic change is observed in % elongation and there is a reduction in this area due to brittle fracture. For r-A1000-AC, % elongation and reduction in the area were measured to be 12% and 21% respectively, which indicated a brittle fracture of material and it occurred due to untempered martensitic microstructure.

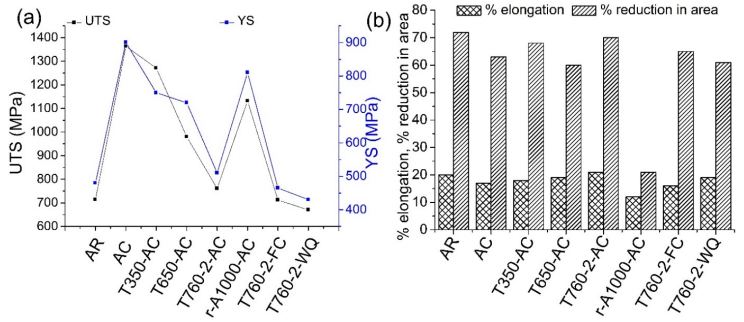


***Fig. 17. Variation in UTS and YS of P92 steel in different heat treatment condition (a, b) showing :***
a – variation in % elongation; b – % reduction in area

### *3.3.5 Hardness and Charpy toughness*

The "as-received" hardness of P92 steel was 247±5 HV. A drastic change was noted in hardness after austenitizing at 1040 ºC for 40 min due to the formation of untempered lath martensite. The austenitizing results in higher solid solution strengthening due to the dissolution of precipitates. The variation in hardness for varying heat treatment condition is shown in Fig. 18. The variation in hardness depends on precipitation hardening, solid solution hardening, fine precipitates density, and dislocation density. In T350-AC condition, hardness value is decreased but not as much as compared to AC state because of negligible precipitation. A noticeable change is observed, as tempering temperature increased from 350 ºC to 650 ºC. Tempering at 650 ºC leads to a reduction in the solid solution strengthening that results in a decrease in the hardness of P92 steel in T650-AC condition compared to T350-AC condition. In T760-2-AC condition, because of fine grain formation, the number of grains

per unit area is increased as compared to the T650-AC condition that provides the precipitate nucleation sites. This resulted in higher area fraction of precipitates in T760-2-AC condition. The increase in the area fraction of precipitates leads to the decrease in hardness because of reduction in solid solution strengthening. The increase in tempering temperature results in higher number of fine precipitates at the surface that might be contributing to the hardness of P92 steel due to precipitation hardening. The precipitation hardening effect is observed to be negligible as compared to solid solution hardening effect. With further increase in tempering temperature from 760 ºC to 1000 ºC, the hardness is observed to be increased due to formation of brittle fresh untempered lath martensite. In r-A1000-AC condition, dissolution of precipitates leads to the formation of untempered lath martensite with a higher weight percentage of C and N. In T760-2-FC condition, slow cooling rate, precipitates and grain coarsening lead to a poor hardness value. In T760-2-WQ state, hardness is observed to be increased because of formation of quenched lath martensite and higher dislocation density. The increase in tempering temperature also leads to the reduction in dislocation density, which might have contributed to variation in hardness with respect to tempering temperature.

Charpy impact toughness value of P92 steel at room temperature was measured to be 198±8. The variation in Charpy toughness value with varying heat treatment condition is shown in Fig. 19. Normalizing of as-received P92 steel (AC) resulted in a drastic decrease in toughness value and it reduced up to 80±6 Joules because of the presence of untempered lath martensite in the microstructure. Tempering of austenitized P92 steel at 350 ºC does not severely affect its toughness value because of partial tempering of the lath martensite and value is measured to be 130±6 Joules. The positive increment in toughness value of P92 is observed after tempering at 650 ºC due to tempering reaction. The maximum value of Charpy toughness is measured to be 220±4.5 Joules in the T760-2-AC state. The lowest value of toughness is observed in r-A1000-AC condition due to the presence of highly brittle fresh untempered martensite. In T760-2-FC and T760-2-WQ conditions, Charpy toughness value is measured to be 165±4 and 148±6 Joules, respectively, which was higher than the toughness value measured in T350-AC condition. The lower toughness value obtained in T760-2-WQ condition indicates the presence of quench martensite. The grain coarsening and cracking of secondary phase carbide particles during thermal straining and decohesion at precipitates and matrix interface might have been responsible for the reduction in toughness value as compared to the T760-2-AC condition.

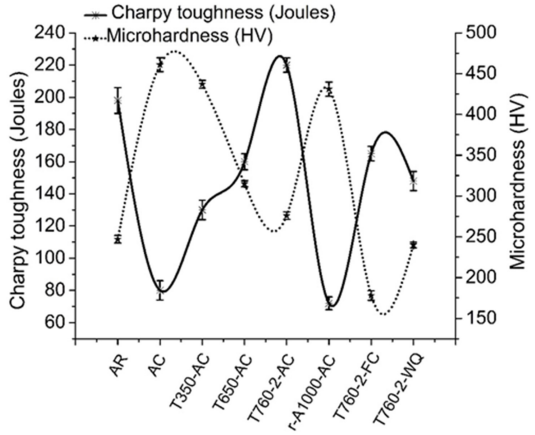


***Fig. 18. Variation in hardness and Charpy toughness of 92 steel in different operating conditions***

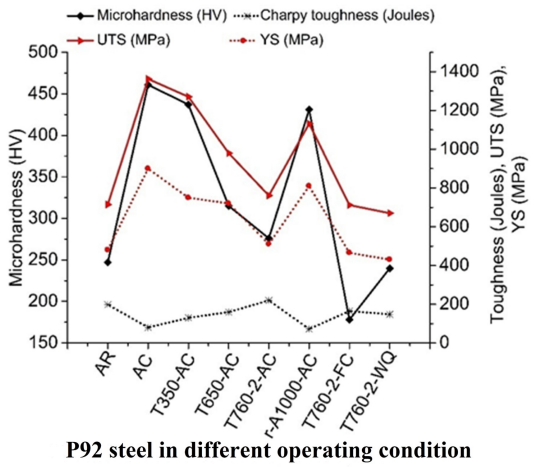


***Fig. 19. Combined effect of various heat treatment conditions on YS, UTS, Charpy toughness, and microhardness of P92 steel***

A combined study has been done to obtain the optimum combination of mechanical properties in different operating conditions. From Fig. 19, it can be inferred that optimum combination of UTS, YS, and hardness was observed in AC s and r-A1000-AC state but at this condition, Charpy toughness is lower, which is the required essential property for P92 steel in operating condition. The other optimum combination of all four properties was noticed at the tempering temperature of 650 ºC and 760 ºC. It was observed that at 650 ºC, toughness was lower and another drawback of the T650-AC condition is lower number density of precipitates as compared to the T760-2-AC state. The fine carbide precipitates present at the sub-grain boundaries and MX precipitates in the matrix are helpful for enhanc-

ing the essential creep strength of P92 steel by pinning the movement of dislocations, PAGBs and sub-grain boundaries. Hence, the optimum combination of mechanical properties is obtained at tempering temperature of 760 ºC, after the austenitizing at 1040 ºC for 40 min.

### *3.4 Effect of varying tempering time*

In the previous study, normalizing and tempering temperature are varied to obtain the enhanced combination of microstructure and mechanical properties. The maximum normalizing temperature was recommended to be about 1050 ºC while tempering at 760 ºC, followed by air cooling. In this section, an initial heat treatment of normalizing at 1040 ºC for 40 min was performed, in order to get the complete martensitic structure. The normalized steel was subjected to tempering at 760 ºC for varying tempering from 2–8 hours for microstructure and mechanical properties analysis. Heat treatment was performed as per Table 7.

#### *3.4.1 Microstructure evolution and precipitate in T760-2-AC, T760-4-AC, T760-6-AC, T760-8-AC conditions*

Effect of varying tempering time on microstructure evolution is shown in Fig. 20. Microstructure reveals the tempered martensitic microstructure that derives its stability from solid solution and precipitation hardening. PAGBs and carbide precipitates are clearly indicated both at lower and higher magnification. The $M_{23}C_6$ appears in the early stages of the tempering process and is usually Cr-rich ($Cr_{23}C_6$). Mo, Mn, and Fe can also form the carbide structure, but Cr carbide is more commonly encountered due to its thermal stability and the relative abundance of chromium in the matrix of the steels concerned. Grain coarsening is clearly observed with increase in tempering time from 2 h to 4 h, as shown in Fig. 20, a, c. During increase in tempering time from 2 h to 4 h, the particle size was not affected so much and it increased from 110±39 nm to 114±42 nm but a reduction in the number density of precipitates is observed due to grain coarsening. In T760-4-AC condition, a great heterogeneity is observed in particle size and it varies from 31 to 251 nm. The grain coarsening leads to the lower precipitation of carbides during tempering because of smaller number of grains per unit area and the reduction in precipitates density, as shown in Fig. 20, b, d, which leads to a reduction in creep strength of the material. During further increase in tempering time from 4 h to 6 h, recrystallization occurs and no grain coarsening is detected, as shown in Fig. 20, c, e, and at the same time formation of new grains leads to higher area fraction of precipitates as shown in Fig. 20, d, f. During increase in tempering time from 4 h to 6 h, grain coarsening was not observed but thermal straining of existing precipitates occurred and particles size increased from 114±42 nm to 121±46 nm. In T760-6-AC condition, particle size varied in the range of 32–257 nm. During further increase in tempering time from 6 h to 8 h, no grain coarsening is observed, as shown in Fig. 20, e, g. The area fraction of precipitates is decreased, which is clearly observed in Fig. 20, f, h. After tempering of 8 h, a drastic increase is observed in particle size and it increases from 121±46 nm to 157±58 nm,

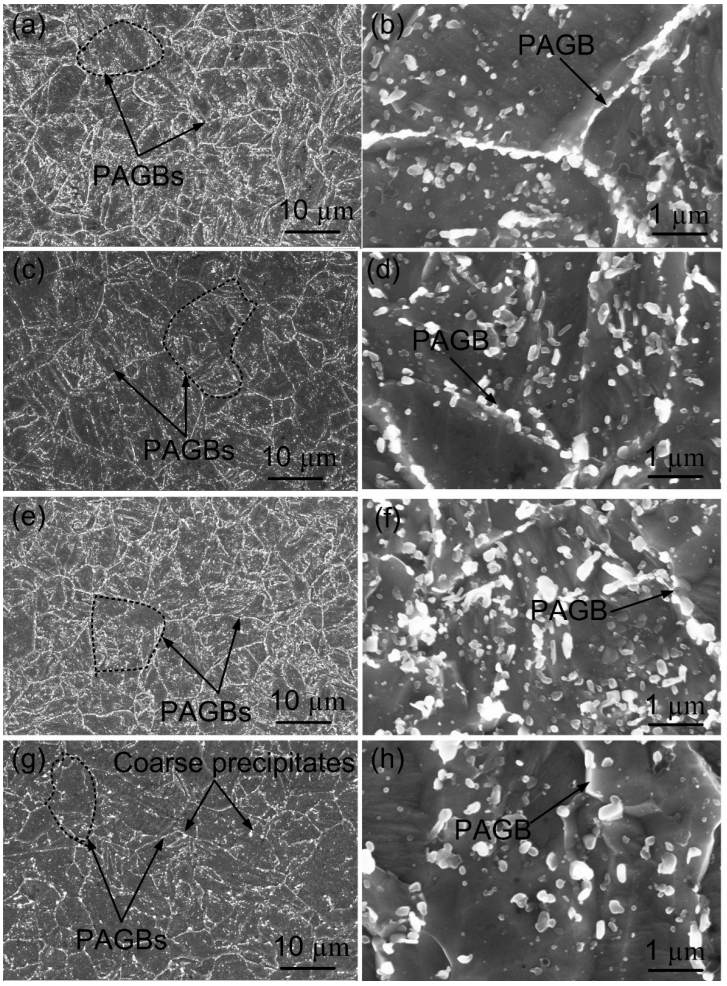


***Fig. 20. Microstructure of P92 steel tempered at 760 ºC for different tempering time and different magnification:***
a – 2 h at 5000x; b – 2 h at 50 Kx; c – 4h at 5000x; d – 4h at 50 Kx; e – 6 h at 5000x; f – 6h at 50 Kx; g – 8 h at 5000x; h – 8 h at 50 Kx

as shown in Fig. 20, b, which is quite harmful in terms of creep strength. In T760-8-AC condition, particle size varied within 38–323 nm. Coarse precipitates in order of 300 nm are also observed from the low magnification micrograph, as shown in Fig. 20, g. Generally, formations of coarse precipitates are observed along PAGBs. Inside the lath matrix region, less density of precipitates is observed as shown in Fig. 20, g.

Effect of tempering time on lath width and interparticle spacing is given in Fig. 20, a. In as-received condition, lath width was measured to be 0.40±.035 μm, which was similar to as reported by Vivas et al. [31].

A great heterogeneity is observed in lath width and interparticle spacing. Lath width remained stable up to tempering time of 4 h and after that, it increased drastically up to 8 h. Tempering time had a small influence on the particle-to-particle distance up to tempering time of 6 h and after that it increased drastically, as shown in Fig. 21, b. To study the effect of varying tempering time on the relative change in the composition of $M_{23}C_6$, Cr/Fe ratio has been evaluated. To quantify the various elements present in $M_{23}C_6$ carbide, the EDS spectra have been taken for various tempering state and plotted in Fig. 21, c. A continuous increase in the Cr/Fe ratio is observed with increase in tempering time from 2 to 8 h. The increase in Cr/Fe ratio with tempering time attributed towards the continuous development of the meta-stable $M_{23}C_6$ phase. Thomas Paul et al. [26] also observed the continuous increase in Cr/Fe ratio during thermal aging with respect to time and temperature.

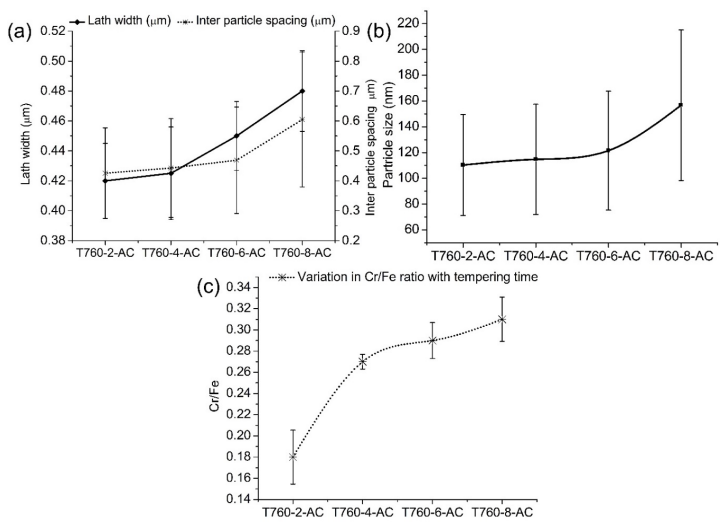


***Fig. 21. Variation in lath width and particle-to-particle distance showing:***
a – variation in precipitate size ;
b – compositional variation of $M_{23}C_6$ carbides;
c – as a function of tempering time

### *3.4.2 Grain size*

A good agreement was obtained for the grain size measured with optical micrograph and SEM, which is shown in Fig. 22. After tempering at 760 ºC for 2 h (T760-2-AC), the tempered martensitic structure with an average austenite grain size of about 39±6 μm is observed, as shown in Fig. 22. The grain size increased from 39±6 μm to 52±8 μm, as shown in Fig. 22. With further increase in tempering time from 4 h to 6 h, no grain coarsening was observed because of formation of new grains, and grain size decreases from 52±8 μm to 48±6 μm. With further increase in tempering time from 6 h to 8 h, there was decrement in grain size from 48±6 μm to 46±8 μm, which was almost similar to the grain size of "as-received" P92 steel.

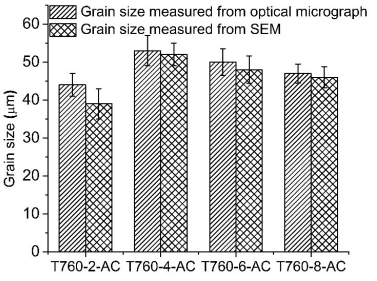


***Fig. 22. Variation in grain size as a function of tempering time***

### *3.4.3 Tempering time effect on mechanical properties*

The variation in yield strength (YS), and ultimate tensile strength (UTS) with tempering time is shown in Fig. 23, a. The YS and UTS were found to be decreasing continuously with increase in tempering time up to 8 h. The extent of decrease in YS and UTS is much higher for tempering time of 8 h. Increase in tempering time from 2 h to 4 h, grain coarsening and lath widening lead to lower precipitation. The grain coarsening resulted in lower precipitation and higher solid solution hardening. However, softening effect due to grain coarsening and thermal straining of precipitates dominates over solid solution strengthening provided by C and N presence in the solution matrix. Increase in tempering time from 4 to 6 h results in the formation of fine grains due to recrystallization. Almost negligible amount of grain coarsening, precipitate coarsening and lath widening lead to a negligible reduction in YS and UTS. A drastic decrease in YS and UTS is observed after tempering up

to 8 h. Tempering up to 8 h results in grain refining that leads to higher precipitation across PAGBs and lath boundaries and considerable lowering in solid solution strengthening. For the same tempering time, a drastic increase in precipitate size is also observed. Hence, lowering in solid solution strengthening and precipitate coarsening might be the cause of the drastic reduction in YS and UTS of P92 steel.

Effect of varying tempering time on microhardness of P92 steel is shown in Fig. 23, b. Microhardness is observed to be decreased with increase in tempering time. The decrease in hardness is attributed to the tempering of martensite and precipitation of $M_{23}C_6$ carbide and fine MX carbonitride particles. After tempering of 2 h, hardness value was measured to be about 276 HV. With increase in tempering time from 2 h to 4 h, a little change in hardness value beyond which a large amount of grain coarsening occurs was noticed. Lower availability of precipitate nucleation sites results in a considerable lower inginfraction area of precipitates that led to solid solution hardening. Increase in solid solution hardening might be the possible cause of the increase in hardness but at the same time, grain coarsening and thermal straining of particles were also observed which results in lowering of hardness value. Grain coarsening and precipitate coarsening dominate the solid solution hardening that resulted in a reduction in hardness for T760-4-AC condition compared to T760-2-AC. The same effect is also observed on further increase in tempering time. Increase in tempering time from 6 h (T760-6-AC) to 8 h (T760-8-AC) results in a drastic decrease in hardness value as shown in Fig. 23, b. It occurs mainly due to softening the effect. The effect of tempering time for tempering temperature of 760 ºC on the room temperature Charpy toughness of P92 steel is shown in Fig. 23, b. Increase in tempering time increases the material energy absorbing capacity up to tempering time of 6 h and after that, it decreases drastically. A decrease in impact toughness value after 6 h of tempering is attributed to cracking of secondary phase carbide particles during thermal straining and decohesion at precipitates and matrix interface. The maximum impact toughness value of P92 steel was observed after tempering of 6 h and it was about 265 Joules, which was much more than the impact toughness value of P92 steel in the as-received state (198 Joules).

A combined study has been done to obtain the optimum combination of mechanical properties, grain size, and precipitates size for varying tempering time at the tempering temperature of 760 ºC. From Fig. 24, it was observed that optimum combination of mechanical properties, grain size, and particle size are obtained for tempering time of 6 h. After 6 h of tempering, precipitates size is observed to be increased, this might be quite harmful in terms of creep strength. Even at 2 h tempering, better combination of mechanical properties was observed, except toughness and high grain size, which reduces the area fraction of carbides precipitates. For the economy purpose, in place of 6 h of tempering, generally 2 h of tempering was performed after austenitizing.

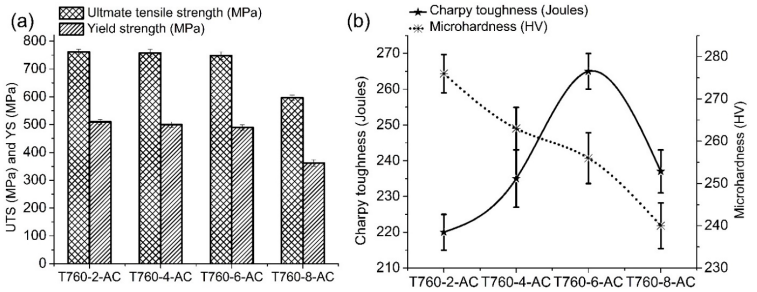


***Fig. 23. Variation in tensile properties with tempering time (a) and variation in Charpy toughness and micro hardness with tempering time (b)***

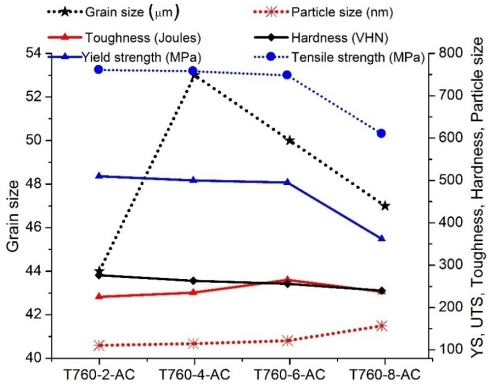


***Fig. 24. Combined effect of tempering time at temperature of 760 ºC on mechanical properties (YS, UTS, Toughness, and Hardness), grain size, and particle size***

## 4. Conclusions

1. The optimum combination of the microstructure and mechanical properties were obtained for normalizing temperature of 1040 ºC with tempering time of 760 ºC.

2. The poor mechanical properties were obtained for the furnace-cooled condition, which was attributed to precipitate and grain coarsening.

3. The reduction in strength and hardness was obtained with increase in tempering temperature, which might be due to tempering reaction which includes the lath break up, reduction in dislocation density and increase in precipitates size and fraction area of the precipitates.

4. In AC and T350 state, a negligible precipitate was observed along the boundaries. However, at higher magnification, fine precipitates of MX type were obtained along the lath blocks and inside the matrix region.

5. The Cr, Fe, Mo and Wo enriched $M_{23}C_6$, $M_7C_3$ and V and Nb enriched Mx type precipitates were obtained.

**References**


1. Klueh, R. L. (2005). Elevated temperature ferritic and martensitic steels and their application to future nuclear reactors. *International Materials Reviews*, vol. 50, iss. 5, pp. 287–310. https://doi.org/10.1179/174328005X41140.
2. Mannan, S. L., Chetal, S. C., Raj, B., & Bhoje, S. B. (2003). Selection of materials for prototype fast breeder reactor. *Transactions of the Indian Institute of Metals*, pp. 1–35.
3. Shrestha, T., Alsagabi, S. F., Charit, I., Potirniche, G. P., & Glazoff, M. V. (2015). Effect of heat treatment on microstructure and hardness of Grade 91 steel. *Metals*, vol. 5, iss. 1, pp. 131–149. https://doi.org/10.3390/met5010131.
4. Golański, G. (2010). Effect of the heat treatment on the structure and properties of GX12CrMoVNbN9-1 cast steel. *Archives of Materials Science and Engineering*, vol. 46, iss. 2, pp. 88–97.
5. Golański, G. & Słania, J. (2013). Effect of different heat treatments on microstructure and mechanical properties of the martensitic GX12CrMoVNbN9-1 cast steel. *Archives of Metallurgy and Materials*, vol. 58, iss. 1, pp. 25–30. https://doi.org/10.2478/v10172-012-0145-x.
6. Jones, W. B., Hills, C. R., & Polonis, D. H. (1991). Microstructural evolution of modified 9Cr-lMo steel. *Metallurgical Transactions A*, vol. 22, pp. 1049–1058. https://doi.org/10.1007/BF02661098.
7. Yoshino, M., Mishima, Y., Toda, Y., Kushima, H., Sawada, K., & Kimura, K. (2008). Influence of normalizing heat treatment on precipitation behavior in modified 9Cr-1Mo steel. *Materials at High Temperatures*, vol. 25, iss. 3, pp. 149–158. https://doi.org/10.3184/096034008X356349.
8. Yoshino, M., Mishima, Y., Toda, Y., Kushima, H., Sawada, K., & Kimura, K. (2005). Phase equilibrium between austenite and MX carbonitride in a 9Cr-1Mo-V-Nb steel. *ISIJ International*, vol. 45, iss. 1, pp. 107–115. https://doi.org/10.2355/isijinternational.45.107.
9. Hurtado-Noreña, C., Danón, C. A., Luppo, M. I., & Bruzzoni, P. (2015). Evolution of minor phases in a P91 steel normalized and tempered at different temperatures. *Procedia Materials Science*, vol. 8, pp. 1089–1098. https://doi.org/10.1016/j.mspro.2015.04.172.
10. Chatterjee, A., Chakrabarti, D., Moitra, A., Mitra, R., & Bhaduri, A. K. (2014). Effect of normalization temperatures on ductile – brittle transition temperature of a modi fi ed 9Cr – 1Mo steel. *Materials Science and Engineering: A*, vol. 618, pp. 219–231. https://doi.org/10.1016/j.msea.2014.09.021.
11. Karthikeyan, T., Dash, M. K., Ravikirana, Mythili, R., Selvi, S. P., Moitra, A., & Saroja, S. (2017) Effect of prior-austenite grain refinement on microstructure, mechanical properties and thermal embrittlement of 9Cr-1Mo-0.1C steel. *Journal of Nuclear Materials*, vol. 494, pp. 260–277. https://doi.org/10.1016/j.jnucmat.2017.07.019.
12. Karthikeyan, T., Paul, V. T., Saroja, S., Moitra, A., Sasikala, G., & Vijayalakshmi, M. (2011). Grain refinement to improve impact toughness in 9Cr-1Mo steel through a double austenitization treatment. *Journal of Nuclear Materials*, vol. 419, iss. 1–3, pp. 256–262. https://doi.org/10.1016/j.jnucmat.2011.08.010.
13. Homolova, V., Janovec, J., Zahumensky, P., & Vyrostkova, A. (2003). Influence of thermal-deformation history on evolution of secondary phases in P91 steel. *Materials Science and Engineering: A*, vol. 349, pp. 306–312. https://doi.org/10.1016/S0921-5093(02)00768-2.
14. Kafexhiu, F., Vodopivec, F., & Tuma, J. V. (2012). Effect of tempering on the room-temperature mechanical properties of X20CrMoV121 and P91 steels. *Materials and Technologies*, vol. 46, iss. 5, pp. 459–464.
15. Senior, B. A., Noble, F. W., & Eyres, B. L. (1988). The effect of ageing on the ductility of 9Cr-l Mo steel. *Acta Metallurgica*, vol. 36, iss. 7, pp. 1855–1862. https://doi.org/10.1016/0001-6160(88)90253-2.
16. Sathyanarayanan, S., Basu, J., Moitra, A., Sasikala, G., & Singh, V. (2013). Effect of thermal aging on ductile-brittle transition temperature of modified 9Cr-1Mo steel evaluated with reference temperature approach under dynamic loading condition. *Metallurgical and Materials Transactions A*, vol. 44, pp. 2141–2155. https://doi.org/10.1007/s11661-012-1510-0.
17. Golański, G. & Kepa, J. (2012). The effect of ageing temperatures on microstructure and mechanical properties of GX12CrMoVNbN9-1 (GP91) cast steel. *Archives of Metallurgy and Materials*, vol. 57, iss. 2, pp. 575–582. https://doi.org/10.2478/v10172-012-0061-0.

18. (2014). ASTM A370-14. Standard test methods and definitions for mechanical testing of steel products. ASTM Int. West Conshohocken, PA. https://doi.org/10.1520/A0370-14.2.
19. Choudhary, B. K., Christopher, J., Palaparti, D. P. R., Samuel, E. I., & Mathew, M. D. (2013). Influence of temperature and post weld heat treatment on tensile stress-strain and work hardening behaviour of modified 9Cr-1Mo steel. *Materials & Design*, vol. 52, pp. 58–66. https://doi.org/10.1016/j.matdes.2013.05.020.
20. Panait, C. G., Zielińska-Lipiec, A., Koziel, T., Czyrska-Filemonowicz, A., Gourgues-Lorenzon, A.-F., & Bendick, W. (2010). Evolution of dislocation density, size of subgrains and MX-type precipitates in a P91 steel during creep and during thermal ageing at 600C for more than 100,000h. *Materials Science and Engineering: A*, vol. 527, iss. 16–17, pp. 4062–4069. https://doi.org/10.1016/j.msea.2010.03.010.
21. Arivazhagan, B. & Kamaraj, M. (2013). Metal-cored arc welding process for joining of modified 9Cr-1Mo. *Journal of Manufacturing Processes*, vol. 15, iss. 4, pp. 542–548. https://doi.org/10.1016/j.jmapro.2013.07.001.
22. Wang, Y., Kannan, R., & Li, L. (2016). Characterization of as-welded microstructure of heat-affected zone in modified 9Cr-1Mo-V-Nb steel weldment. *Materials Characterization*, vol. 118, pp. 225–234. https://doi.org/10.1016/j.matchar.2016.05.024.
23. Baltusnikas, A., Levinskas, R., & Lukošiute, I. (2007). Kinetics of carbide formation during ageing of pearlitic 12X1M phi Steel. *Materials Science*, vol. 13, pp. 286–292.
24. Hurtado-Noren, C., Danon, C. A., Luppo, M. I., & Bruzzoni, P. (2015). Evolution of minor phases in a 9PctCr steel : Effect of tempering temperature and relation with hydrogen trapping. *Metallurgical and Materials Transactions A*, vol. 46, pp. 3972–3988. https://doi.org/10.1007/s11661-015-3045-7.
25. Maruyama, K., Sawada, K., & Koike, J. (2001) Strengthening mechanisms of creep resistant tempered martensitic steel. *ISIJ International*, vol. 41, iss. 6, pp. 641–653. https://doi.org/10.2355/isijinternational.41.641.
26. Paul, V. T., Saroja, S., & Vijayalakshmi, M. (2008). Microstructural stability of modified 9Cr–1Mo steel during long term exposures at elevated temperatures. *Journal of Nuclear Materials*, vol. 378, iss. 3, pp. 273–281. https://doi.org/10.1016/j.jnucmat.2008.06.033.
27. Yan, W., Wang, W., Shan, Y. Y., & Yang, K. (2013). Microstructural stability of 9-12%Cr ferrite/martensite heat-resistant steels. *Frontiers of Materials Science*, vol. 7, pp. 1–27. https://doi.org/10.1007/s11706-013-0189-5.
28. Vodopivec, F., Kmetic, D., Vojvodi-Tuma, J., & Skobir, D. A. (2004). Effect of operating temperature on microstructure and creep resistance of X20CrMoV121 steel. *Materiali in Tehnologije*, vol. 38, iss. 5, pp. 233–239.
29. Thakur, S. K. & Dhindaw, B. K. (2001). Influence of interfacial characteristics between $SiC_p$ and Mg/Al metal matrix on wear, coefficient of friction and microhardness. *Wear*, vol. 247, pp. 191–201. https://doi.org/10.1016/S0043-1648(00)00536-6.
30. Thakur, S. K. & Gupta, M. (2007). Improving mechanical performance of Al by using Ti as reinforcement. *Composites Part A: Applied Science and Manufacturing*, vol. 38, iss. 3, pp. 1010–1018. https://doi.org/10.1016/j.compositesa.2006.06.014.
31. Vivas, J., Capdevila, C., Jimenez, J. A., Benito-Alfonso, M., & San-Martin, D. (2017). Effect of ausforming temperature on the microstructure of G91 steel. *Metals*, vol. 7, iss. 7, pp. 1–11. https://doi.org/10.3390/met7070236.

*Received 05 May 2022*

## Вплив різних режимів термічної обробки на мікроструктуру та механічні властивості сталевих швів типу P92

**Vinay Kumar Pal, Lokendra Pal Singh**

Факультет машинобудування, Університет сільського господарства, технологій і наук Сема Хіггінботтома, Аллахабад, 211007, Уттар-Прадеш, Індія

*Сталі типу Cr-Mo добре відомі своїм високотемпературним застосуванням на теплових електростанціях. P91, P911 і P92 є найбільш часто використовуваними сталями типу Cr-Mo, розрахованими на високі температури. Сталі отримали свою міцність від загартованого мартенситу та осадів типу MX та $M_{23}C_6$. Перед приведенням сталей у робочий стан були проведені їх нормалізація та загартовування. У цьому рукописі описано вплив різних режимів термічної обробки на мікроструктуру та механічні властивості сталі P92. Досліджено вплив нормалізації на мікроструктуру та механічні властивості. Нормалізація була проведена в діапазоні 950-1150 °C. Також було вивчено вплив різного часу гартування на механічну поведінку сталі P92 і докладено зусиль для встановлення зв'язку між мікроструктурою та механічними властивостями. Для дослідження мікроструктури використовувалися оптичний і скануючий електронний мікроскопи. Для охарактеризування механічної поведінки були проведені випробування на розтяг, твердість та ударну в'язкість за Шарпі.*

***Ключові слова:*** *P92, мікроструктура, механічні властивості, нормалізація, загартування.*

**Література**


1. Klueh R. L. Elevated temperature ferritic and martensitic steels and their application to future nuclear reactors. *International Materials Reviews*. 2005. Vol. 50. Iss. 5. P. 287–310. https://doi.org/10.1179/174328005X41140.
2. Mannan S. L., Chetal S. C., Raj B., Bhoje S. B. Selection of materials for prototype fast breeder reactor. *Transactions of the Indian Institute of Metals*. 2003. P. 1–35.
3. Shrestha T., Alsagabi S. F., Charit I., Potirniche G. P., Glazoff M. V. Effect of heat treatment on microstructure and hardness of Grade 91 steel. *Metals.* 2015. Vol. 5. Iss. 1. P. 131–149. https://doi.org/10.3390/met5010131.
4. Golański G. Effect of the heat treatment on the structure and properties of GX12CrMoVNbN9-1 cast steel. *Archives of Materials Science and Engineering*. 2010. Vol. 46. Iss. 2. P. 88–97.
5. Golański G., Słania J. Effect of different heat treatments on microstructure and mechanical properties of the martensitic GX12CrMoVNbN9-1 cast steel. *Archives of Metallurgy and Materials*. 2013. Vol. 58. Iss. 1. P. 25–30. https://doi.org/10.2478/v10172-012-0145-x.
6. Jones W. B., Hills C. R., Polonis D. H. Microstructural evolution of modified 9Cr-lMo steel. *Metallurgical Transactions A*. 1991. Vol. 22. P. 1049–1058. https://doi.org/10.1007/BF02661098.
7. Yoshino M., Mishima Y., Toda Y., Kushima H., Sawada K., Kimura K. Influence of normalizing heat treatment on precipitation behavior in modified 9Cr-1Mo steel. *Materials at High Temperatures*. 2008. Vol. 25. Iss. 3. P. 149–158. https://doi.org/10.3184/096034008X356349.
8. Yoshino M., Mishima Y., Toda Y., Kushima H., Sawada K., Kimura K. Phase equilibrium between austenite and MX carbonitride in a 9Cr-1Mo-V-Nb steel. *ISIJ International*. 2005. Vol. 45. Iss. 1. P. 107–115. https://doi.org/10.2355/isijinternational.45.107.
9. Hurtado-Noreña C., Danón C. A., Luppo M. I., Bruzzoni P. Evolution of minor phases in a P91 steel normalized and tempered at different temperatures. *Procedia Materials Science*. 2015. Vol. 8. P. 1089–1098. https://doi.org/10.1016/j.mspro.2015.04.172.
10. Chatterjee A., Chakrabarti D., Moitra A., Mitra R., Bhaduri A. K. Effect of normalization temperatures on ductile – brittle transition temperature of a modi fi ed 9Cr – 1Mo steel. *Materials Science and Engineering: A*. 2014. Vol. 618. P. 219–231. https://doi.org/10.1016/j.msea.2014.09.021.
11. Karthikeyan T., Dash M. K., Ravikirana, Mythili R., Selvi S. P., Moitra A., Saroja S. Effect of prior-austenite grain refinement on microstructure, mechanical properties and thermal embrittlement of 9Cr-1Mo-0.1C steel. *Journal of Nuclear Materials*. 2017. Vol. 494. P. 260–277. https://doi.org/10.1016/j.jnucmat.2017.07.019.
12. Karthikeyan T., Paul V. T., Saroja S., Moitra A., Sasikala G., Vijayalakshmi M. Grain refinement to improve impact toughness in 9Cr-1Mo steel through a double austenitization treatment. *Journal of Nuclear Materials*. 2011. Vol. 419. Iss. 1–3. P. 256–262. https://doi.org/10.1016/j.jnucmat.2011.08.010.
13. Homolova V., Janovec J., Zahumensky P., Vyrostkova A. Influence of thermal-deformation history on evolution of secondary phases in P91 steel. *Materials Science and Engineering: A*. 2003. Vol. 349. P. 306–312. https://doi.org/10.1016/S0921-5093(02)00768-2.
14. Kafexhiu F., Vodopivec F., Tuma J. V. Effect of tempering on the room-temperature mechanical properties of X20CrMoV121 and P91 steels. *Materials and Technologies*. 2012. Vol. 46. Iss. 5. P. 459–464.
15. Senior B. A., Noble F. W., Eyres B. L. The effect of ageing on the ductility of 9Cr-l Mo steel. *Acta Metallurgica*. 1988. Vol. 36. Iss. 7. P. 1855–1862. https://doi.org/10.1016/0001-6160(88)90253-2.
16. Sathyanarayanan S., Basu J., Moitra A., Sasikala G., Singh V. Effect of thermal aging on ductile-brittle transition temperature of modified 9Cr-1Mo steel evaluated with reference temperature approach under dynamic loading condition. *Metallurgical and Materials Transactions A*. 2013. Vol. 44. P. 2141–2155. https://doi.org/10.1007/s11661-012-1510-0.
17. Golański G., Kepa J. The effect of ageing temperatures on microstructure and mechanical properties of GX12CrMoVNbN9-1 (GP91) cast steel. *Archives of Metallurgy and Materials*. 2012. Vol. 57. Iss. 2. P. 575–582. https://doi.org/10.2478/v10172-012-0061-0.
18. (2014). ASTM A370-14. Standard test methods and definitions for mechanical testing of steel products. ASTM Int. West Conshohocken, PA. https://doi.org/10.1520/A0370-14.2.
19. Choudhary B. K., Christopher J., Palaparti D. P. R., Samuel E. I., Mathew M. D. Influence of temperature and post weld heat treatment on tensile stress-strain and work hardening behaviour of modified 9Cr-1Mo steel. *Materials & Design*. 2013. Vol. 52. P. 58–66. https://doi.org/10.1016/j.matdes.2013.05.020.
20. Panait C. G., Zielińska-Lipiec A., Koziel T., Czyrska-Filemonowicz A., Gourgues-Lorenzon A.-F., Bendick W. Evolution of dislocation density, size of subgrains and MX-type precipitates in a P91 steel during creep and during thermal ageing at 600C for more than 100,000h. *Materials Science and Engineering: A*. 2010. Vol. 527. Iss. 16–17. P. 4062–4069. https://doi.org/10.1016/j.msea.2010.03.010.

21. Arivazhagan B., Kamaraj M. Metal-cored arc welding process for joining of modified 9Cr-1Mo. *Journal of Manufacturing Processes*. 2013. Vol. 15. Iss. 4. P. 542–548. https://doi.org/10.1016/j.jmapro.2013.07.001.
22. Wang Y., Kannan R., Li L. Characterization of as-welded microstructure of heat-affected zone in modified 9Cr-1Mo-V-Nb steel weldment. *Materials Characterization*. 2016. Vol. 118. P. 225–234. https://doi.org/10.1016/j.matchar.2016.05.024.
23. Baltusnikas A., Levinskas R., Lukošiute I. Kinetics of carbide formation during ageing of pearlitic 12X1M phi steel. *Materials Science*. 2007. Vol. 13. P. 286–292.
24. Hurtado-Noren C., Danon C. A., Luppo M. I., Bruzzoni P. Evolution of minor phases in a 9PctCr steel : Effect of tempering temperature and relation with hydrogen trapping. *Metallurgical and Materials Transactions A*. 2015. Vol. 46. P. 3972–3988. https://doi.org/10.1007/s11661-015-3045-7.
25. Maruyama K., Sawada K., Koike J. Strengthening mechanisms of creep resistant tempered martensitic steel. *ISIJ International*. 2001. Vol. 41. Iss. 6. P. 641–653. https://doi.org/10.2355/isijinternational.41.641.
26. Paul V. T., Saroja S., Vijayalakshmi M. Microstructural stability of modified 9Cr–1Mo steel during long term exposures at elevated temperatures. *Journal of Nuclear Materials*. 2008. Vol. 378. Iss. 3. P. 273–281. https://doi.org/10.1016/j.jnucmat.2008.06.033.
27. Yan W., Wang W., Shan Y. Y., Yang K. Microstructural stability of 9-12%Cr ferrite/martensite heat-resistant steels. *Frontiers of Materials Science*. 2013. Vol. 7. P. 1–27. https://doi.org/10.1007/s11706-013-0189-5.
28. Vodopivec F., Kmetic D., Vojvodi-Tuma J., Skobir D. A. Effect of operating temperature on microstructure and creep resistance of X20CrMoV121 steel. *Materiali in Tehnologije*. 2004. Vol. 38. Iss. 5. P. 233–239.
29. Thakur S. K., Dhindaw B. K. Influence of interfacial characteristics between $SiC_p$ and Mg/Al metal matrix on wear, coefficient of friction and microhardness. *Wear*. 2001. Vol. 247. P. 191–201. https://doi.org/10.1016/S0043-1648(00)00536-6.
30. Thakur S. K., Gupta M. Improving mechanical performance of Al by using Ti as reinforcement. *Composites Part A: Applied Science and Manufacturing*. 2007. Vol. 38. Iss. 3. P. 1010–1018. https://doi.org/10.1016/j.compositesa.2006.06.014.
31. Vivas J., Capdevila C., Jimenez J. A., Benito-Alfonso M., San-Martin D. Effect of ausforming temperature on the microstructure of G91 steel. *Metals*. 2017. Vol. 7. Iss. 7. P. 1–11. https://doi.org/10.3390/met7070236.